**Biogeosciences
Discussions**

The Jena Diversity-Dynamic Global Vegetation Model (JeDi-DGVM): a diverse approach to representing terrestrial biogeography and biogeochemistry based on plant functional trade-offs

R. Pavlick[1,2], D. T. Drewry[1,3], K. Bohn[1], B. Reu[1,4], and A. Kleidon[1]

[1]Max Planck Institute for Biogeochemistry, Jena, Germany
[2]International Max Planck Research School on Earth System Modelling, Hamburg, Germany
[3]Jet Propulsion Laboratory, California Institute of Technology, Pasadena, California, USA
[4]Institute of Biology, University of Leipzig, Leipzig, Germany

Correspondence to: R. Pavlick (rpavlick@bgc-jena.mpg.de)

Abstract

Dynamic Global Vegetation Models (DGVMs) typically abstract the immense diversity of vegetation forms and functioning into a relatively small set of predefined semi-empirical Plant Functional Types (PFTs). There is growing evidence, however, from the
field ecology community as well as from modelling studies that current PFT schemes
may not adequately represent the observed variations in plant functional traits and
their effect on ecosystem functioning. In this paper, we introduce the Jena Diversity
DGVM (JeDi-DGVM) as a new approach to global vegetation modelling with a richer
representation of functional diversity than traditional modelling approaches based on
a small number of fixed PFTs.

JeDi-DGVM simulates the performance of a large number of randomly-generated
plant growth strategies (PGSs), each defined by a set of 15 trait parameters which
characterize various aspects of plant functioning including carbon allocation, ecophysiology and phenology. Each trait parameter is involved in one or more functional trade-offs. These trade-offs ultimately determine whether a PGS is able to survive under the
climatic conditions in a given model grid cell and its performance relative to the other
PGSs. The biogeochemical fluxes and land-surface properties of the individual PGSs
are aggregated to the grid cell scale using a mass-based weighting scheme.

Simulated global biogeochemical and biogeographical patterns are evaluated
against a variety of field and satellite-based observations following a protocol established by the Carbon-Land Model Intercomparison Project. The land surface fluxes
and vegetation structural properties are reasonably well simulated by JeDi-DGVM,
and compare favorably with other state-of-the-art terrestrial biosphere models. This
is despite the parameters describing the ecophysiological functioning and allometry of
JeDi-DGVM plants evolving as a function of vegetation survival in a given climate, as
opposed to typical approaches that fix land surface parameters derived from observational datasets for each PFT. The approach implemented here in JeDi-DGVM sets
the foundation for future applications that will explore the impacts of explicitly resolving

diverse plant communities, allowing for a more flexible temporal and spatial representation of the structure and function of the terrestrial biosphere.

1 Introduction

Human activities are altering the terrestrial biosphere at a large scale and an alarming rate (Millennium Ecosystem Assessment, 2005). The risks associated with these activities have led to the development of Dynamic Global Vegetation Models (DGVMs; e.g. Foley et al., 1996; Friend et al., 1997; Woodward et al., 1998; Cox, 2001; Sitch et al., 2003). These mechanistic, process-based, numerical models simulate the large-scale dynamics of terrestrial ecosystems and have proven useful for testing hypotheses and making predictions regarding the responses of ecosystem structure and functioning to past and future environmental changes (see recent review by Quillet et al., 2010). DGVMs have also been embedded within comprehensive Earth System Models (ESMs) to capture biogeochemical (e.g. Cox et al., 2000) and biogeophysical (e.g. Foley et al., 2000) feedbacks between the terrestrial biosphere and the physical climate system. Intercomparison studies (Friedlingstein et al., 2006; Sitch et al., 2008), however, have revealed considerable divergence among the results of these models with respect to the fate of the terrestrial biosphere and its function as a driver of the global carbon cycle under projected scenarios of climate change. This divergence may be, at least in part, due to their coarse and differing treatment of plant functional diversity (Sitch et al., 2008; Harrison et al., 2010; R. Fisher et al., 2010).

For reasons of computational efficiency as well as a lack of sufficient data and theory, global vegetation models typically represent the immense functional diversity of the over 300 000 documented plant species to a small number (typically between 4 and 20) of discrete Plant Functional Types (PFTs; Kattge et al., 2011) which are defined a priori before any simulations are run. In the context of DGVMs, PFTs represent broad biogeographical, morphological, and phenological aggregations (e.g. tropical broadleaf evergreen forest or boreal needleleaf deciduous forest) within which parameter values

Jena Diversity DGVM

R. Pavlick et al.

Title Page

Abstract | Introduction

Conclusions | References

Tables | Figures

◀ | ▶

◀ | ▶

Back | Close

Full Screen / Esc

Printer-friendly Version

Interactive Discussion

are held spatially and temporally constant and responses to physical and biotic factors are assumed to be similar (Prentice et al., 2007). They have typically been classified subjectively using expert knowledge and their occurence within a given model grid cell is based, either directly or indirectly, on semi-empirical bioclimatic limits, such as mini-
5 mum or maximum annual temperature (e.g. Box, 1996; Bonan et al., 2002; Sitch et al., 2003). Inductive approaches have also been proposed wherein PFTs are objectively classified by applying statistical techniques to large datasets of vegetation traits and climatic variables (e.g. Chapin et al., 1996; Wang and Price, 2007). Regardless of approach, the PFT schemes used by current DGVMs have been criticized as ad hoc and
10 as ignoring much of our growing knowledge of comparative plant ecology (Harrison et al., 2010).

In fact, the field ecology community has shown that for many plant traits there is a large amount of variation within PFTs, and that for several important traits, there is greater variation within PFTs than between PFTs (Wright et al., 2005; Reich et al.,
15 2007; Kattge et al., 2011). This trait variation may play an important role for many ecosystem functions (Díaz and Cabido, 2001; Westoby et al., 2002; Ackerly and Cornwell, 2007) and for ecosystem resilience to environmental change (Díaz et al., 2006). Recent model-data assimilation studies using eddy covariance fluxes (Groenendijk et al., 2011) as well as other field and satellite-based observations (Alton, 2011) provide
20 confirmation that current PFT schemes are insufficient for representing the full variability of vegetation parameters necessary to accurately represent carbon cycle processes. A more theoretical study by Kleidon et al. (2007) demonstrated that using a small number of discrete vegetation classes in a coupled climate-vegetation model can lead to potentially unrealistic multiple steady-states when compared with a more continuous
25 representation of vegetation. Others have contended that DGVMs may overestimate the negative effects of climate change by not accounting for potential shifts in ecosystem compositions towards species with traits more suited to the new conditions (Purves and Pacala, 2008; Tilman et al., 2006). For example, some coupled climate-vegetation models (e.g. Cox et al., 2000) project an alarming dieback of the Amazon rainforest

under plausible scenarios of continuing anthropogenic greenhouse gas emissions. The coarse representation of functional diversity in these models provided by current PFT schemes could be leading to an overestimation of the strength and abruptness of this response (R. Fisher et al., 2010). Likewise, DGVMs might underestimate the pos-
5 itive effects of environmental changes on ecosystem performance, e.g. by ignoring warm-adapted species in typically temperature-limited regions (Loehle, 1998). There- fore, while PFTs have been and will likely continue to be useful for many modelling applications, going forward we will need new approaches that allow for a richer repre- sentation of functional diversity in DGVMs.
10 Many approaches have been proposed to meet the challenge of improving the repre- sentation of functional diversity in DGVMs (e.g. Wright et al., 2005; Reich et al., 2007; Kattge et al., 2009; Harrison et al., 2010). However, so far, most of these have apply- ing empirical relationships between observed plant traits and environmental (primarily climatic) factors. The utility of such correlational approaches for predicting the effects
15 of global change on the terrestrial biosphere may be limited, as climate model projec- tions point towards the possibility of novel climates without modern or paleo analogs (Jackson and Williams, 2004; Williams and Jackson, 2007). Other modellers have in- troduced schemes in which PFT parameters adapt to environmental conditions; e.g. with adaptive parameters related to leaf nitrogen (Zaehle and Friend, 2010), allocation
20 (Friedlingstein et al., 1999), and phenology (Scheiter and Higgins, 2009). However, de- spite some interesting proposals (e.g. Falster et al., 2010; Van Bodegom et al., 2011), so far no DGVM has sought to mechanistically represent the full range of functional trait diversity within plant communities (i.e. at the sub-grid scale) using a trait-based trade- off approach. Similar approaches have enabled significant progress in modelling the
25 biogeographical and biogeochemical patterns of global marine ecosystems (Brugge- man and Kooijman, 2007; Litchman et al., 2007; Follows et al., 2007; Dutkiewicz et al., 2009; Follows and Dutkiewicz, 2011)

Here, we introduce our prototype for a new class of vegetation models that mech- anistic resolve sub-grid scale trait variability using functional trade-offs, the Jena

Jena Diversity DGVM

R. Pavlick et al.

Diversity DGVM (hereafter JeDi-DGVM). Just as the first generation of PFT-based DGVMs were built upon earlier PFT-based equilibrium biogeography models, JeDi-DGVM builds upon an equilibrium biogeography model (Kleidon and Mooney, 2000, hereafter KM2000) based on the concept of functional trade-offs and environmental fil-

5 tering. JeDi-DGVM and KM2000 were inspired by the hypothesis "Everything is every-where, but the environment selects!" (Baas-Becking, 1934; O'Malley, 2007). This nearly century-old idea from marine microbiology postulates that all species (or in the case of JeDi-DGVM, combinations of trait parameter values) are, at least latently, present in all places, and that the relative abundances of those species are determined by

10 the local environment based on selection pressures. Rather than simulating a hand-ful PFTs, JeDi-DGVM simulates the performance of a large number of plant growth strategies, which are defined by a vector of 15 functional trait parameters. The trait pa-rameter values determine plant behavior in terms of carbon allocation, ecophysiology, and phenology and are randomly selected from their complete theoretical or observed

15 ranges. JeDi-DGVM is constructed such that each trait parameter is involved in one or more functional trade-offs (Bloom et al., 1985; Smith and Huston, 1989; Hall et al., 1992; Westoby and Wright, 2006). These trade-offs ultimately determine which growth strategies are able to survive under the climatic conditions in a given grid cell as well as their relative biomasses.

20 KM2000 demonstrated that this bottom-up plant functional trade-off approach is ca-pable of reproducing the broad geographic distribution of plant species richness. More recently, their approach has provided mechanistic insight into other biogeographical phenomena including the global patterns of present-day biomes (Reu et al., 2010), community evenness and relative abundance distributions Kleidon et al. (2009), as

25 well as possible mechanisms for biome shifts and biodiversity changes under scenar-ios of global warming (Reu et al., 2011). JeDi-DGVM extends the KM2000 modelling approach to a population-based model capable of representing the large-scale dynam-ics of terrestrial vegetation and associated biogeochemical fluxes by aggregating the

fluxes from the many individual growth strategies following the "biomass-ratio" hypothesis (Grime, 1998).

In the following section, we describe the novel features of the JeDi-DGVM including how functional diversity has been implemented via mechanistic trade-offs and how the resulting fluxes and land-surface properties associated with many plant growth strategies are aggregated to the ecosystem-scale. More detailed descriptions of the model equations and parameters are provided in the Appendices. We then evaluate the simulated patterns of terrestrial biogeochemical fluxes and associated land-surface properties by comparison with a variety of field and satellite-based observations. The model evaluation follows a systematic protocol established by the Carbon-Land Model Intercomparison Project (C-LAMP; Randerson et al., 2009). By following this protocol, we are also able to directly compare the bottom-up functional trade-off approach of JeDi-DGVM with evaluation results for terrestrial biosphere models based on the dominant PFT paradigm. We also evaluate the simulated biogeographical patterns of functional richness and relative abundances to illustrate the parsimonious nature of a functional trade-off approach to dynamic global vegetation modelling, i.e. it can provide more types of testable outputs with fewer inputs. Finally, we discuss the current limitations of the JeDi-DGVM as well as some potential improvements and applications in Sect. 5, before we close with a summary and conclusion.

2   The Jena Diversity-Dynamic Global Vegetation Model

JeDi-DGVM consists of a plant growth module that is coupled tightly to a land surface module. Both components contain parameterizations of ecophysiological and land surface processes that are common to many current global vegetation and land surface models. The main novelties in the vegetation component are (i) an explicit representation of trade-offs that are associated with the diverse set of plant growth strategies, (ii) an inclusion of the whole trait space for testing their relative fitness, and (iii) the aggregation of individual trait combinations based on their relative abundances to grid-scale

structure and function. The following overview of the model focuses on describing the novel combination of these components and how they are implemented in the model, while the full description with the detailed parameterizations are described in the Appendices. A schematic diagram of the JeDi-DGVM modelling approach is shown in Fig. 1.

2.1 Representation of trade-offs

When we speak of terrestrial vegetation, we speak of a large number of plants of different species that differ to some extent in how they grow and respond to the environment. In fact, in a given environment there are potentially many different strategies by which individual plant species could grow and cope with the environment, with some ways being more beneficial to growth and reproductive success than other ways. Some plant species, for instance, grow and reproduce rapidly, such as grasses, while others, such as trees, grow slowly and it takes them a long time to reproduce. Some species allocate a greater proportion of their assimilates to leaves, thereby able to capture more of the incoming sunlight, while others allocate more to root growth and thereby being able to access more moisture within the soil. Some species react quickly to a change in environmental conditions, thereby potentially able to exploit more of the beneficial conditions for growth, while others are more conservative, thereby potentially avoiding damage by a turn to less favorable conditions.

To represent this flexibility of how to grow and reproduce in the model, many different plant growth strategies are simulated simultaneously using the same ecophysiological parameterizations under the same atmospheric forcing. The only part in which the plant growth strategies differ is in their values for fifteen functional trait parameters (Table C2). These parameters control the amount of carbon from photosynthesis and storage allocated to six plant carbon pools (allocation), the response times to changes in environmental conditions and turnover times of the various carbon pools (phenology), and other aspects of ecophysiological functioning (e.g. leaf nitrogen concentration, which determines the balance between photosynthesis and respiration).

Each growth strategy is represented by six carbon pools representing leaves, fine roots, aboveground and belowground wood (stems and coarse roots), storage, and reproduction ("seeds"). These compartments are linked to the physical functioning of the land surface in terms of the absorption of solar radiation and soil moisture dynamics, which are simulated by the land surface module. For instance, leaf biomass is linked to the amount of absorbed solar radiation, and fine root biomass to the capability of a growth strategy to extract soil moisture from the rooting zone. Both of these examples have functional consequences: more absorbed radiation enhances the supply of energy for photosynthesis and evapotranspiration, and the amount of extracted soil water determines the water status of the plant and the supply of moisture for evapotranspiration. This coupled plant-land surface model is therefore capable of simulating the interaction between development of a plant growth strategy and land surface functioning in a process-based manner.

Each trait parameter is associated with costs and benefits, leading to functional trade-offs because no trait value (or set of trait values) can be optimal for plant fitness in all environments. For example, a particular growth strategy may allocate a relatively high fraction of carbon to fine roots, enhancing the rate at which it can extract moisture from the soil matrix. This may be beneficial in terms of higher productivity. However, it is also comes with both real and potential costs. That growth strategy would incur the real metabolic costs of growth and maintenance respiration for the additional fine root biomass. A higher fractional allocation to fine roots also necessarily results in a lower fractional allocation to the other carbon pools (e.g. a lower allocation to the aboveground pools and thus a decreased ability to capture light). In a given environment, there will be some optimum allocation strategy that maximizes productivity. However, in environments with plentiful sunlight and soil moisture, a wide range of allocation strategies will perform close to the optimum. As the climate becomes harsher, the range of well-performing strategies will decrease.

Back | Close

Full Screen / Esc

Printer-friendly Version

Interactive Discussion

2.2 Environmental selection

In order to implement the notion that "everything is everywhere, but the environment selects", we test essentially the complete range of potential values for each of the 15 trait parameters. For some trait parameters, we sample values from the full mathe-
5 matically possible range. For example, the trait parameters controlling the fractional allocation of carbon to the different plant carbon pools are only constrained such that together they sum to one. For other trait parameters (e.g. leaf nitrogen concentration), we sample values from observed ranges taken from literature. To effectively implement environmental selection, the model generates a large number of plant growth strate-
10 gies using a quasi-random Latin Hypercube sampling algorithm (McKay et al., 1979). A 15-dimensional hypervolume representing the potential trait space is first divided into many equal subvolumes. A random point defining a plant growth strategy is then selected from each subvolume.

Each grid cell is seeded with a small amount of initial seed biomass for each plant
15 growth strategy. The model mechanistically simulates the development of the plant growth strategies and their interactions with the coupled land surface module. Growth strategies which are able to maintain a positive balance of stored assimilates survive, passing through what Webb et al. (2010) refers to as a "mechanistic performance fil-ter". As environmental conditions change, different strategies will respond in different
20 ways, some may become more productive, others may no longer able to cope with new conditions and die out. Strategies which were previously filtered out will again be given small amounts of seed carbon and may persist under the new conditions. This process allows the composition of the plant communities in each grid cell to adapt through time, without relying on a priori bioclimatic limits relating the presence or absence of a growth
25 strategy to environmental variables. This mechanistic trial-and-error approach seems potentially better suited to simulate the response of the biosphere to climates with-out present-day analogs because even under new conditions fundamental functional trade-offs that all plants face are unlikely to change.

2.3 Aggregation to ecosystem scale

Some mechanism is needed to aggregate the biogeochemical fluxes and vegetation properties of the potentially many surviving growth strategies within each grid cell. Most current DGVMs calculate grid-cell fluxes and properties as weighted averages across
5 fractional coverages of PFTs. Of those models, the competition between PFTs for fractional area in a grid cell is typically computed implicitly based on moving averages of bioclimatic limits (Arora and Boer, 2006). This approach is not suitable for JeDi-DGVM because its trade-off-based framework does not rely on a priori bioclimatic limits. A few DGVMs (e.g. Cox, 2001; Arora and Boer, 2006) calculate PFT fractional coverages
10 using a form of the Lotka-Volterra equations, in which the colonization rate of each of N PFTs is linked through a N-by-N matrix of competition coefficients. For JeDi-DGVM, this Lotka-Volterra approach quickly becomes computationally burdensome as the size of the necessary competition matrix increases with the square of the potentially large number of tested growth strategies. The necessary competition coefficients are also
15 difficult to determine theoretically (McGill et al., 2006).

Instead, JeDi-DGVM aggregates vegetation fluxes and properties to the grid-cell scale following the "biomass-ratio" hypothesis (Grime, 1998), which postulates that the immediate effects of the functional traits of a species are closely proportional to the relative contribution of that species to the total biomass of the community. Recent work
20 (e.g. Garnier et al., 2004; Vile et al., 2006; Kazakou et al., 2006; Díaz et al., 2007; Quetier et al., 2007) supporting the "biomass-ratio" hypothesis has shown strong statistical links between community-weighted functional traits (i.e. the mean trait values of all species in a community, weighted by their mass-based relative abundances) and observed ecosystem functions (e.g. aboveground net primary productivity and litter
25 decomposition). Others have combined the concept of community-weighted functional traits with the Maximum Entropy (MaxEnt) formalism from statistical mechanics to successfully make predictions, in the other direction, about the relative abundances of

individual species within communities (e.g. Shipley et al., 2006b; Sonnier et al., 2010; Laughlin et al., 2011).

Here, rather than weighting the functional traits, JeDi-DGVM calculates ecosystem-scale variables by directly averaging the fluxes and properties across all surviving growth strategies, weighting the contribution of each strategy by its current biomass relative to the total biomass of all strategies within that grid cell (see Appendix A9 for more details). The resulting ecosystem-scale variables are for the most part diagnostic and do not influence the development of the individual growth strategies or their environmental conditions. Although, the community-aggregated litter fluxes do form the input for a relatively simple soil carbon module, which then provides simulated estimates of heterotrophic respiration (see Appendix A10). This implementation of the "biomass-ratio" hypothesis assumes that interactions between plants, both competitive and facilitative, are weak and do not significantly alter plant survival or relative fitness. The potential implications of this assumption are discussed in Sect. 5.3. In principle, the trait parameters of the surviving growth strategies could also be aggregated, forming an additional testable output of the model. This is discussed further in Sect. 5.4.

3 Methods

3.1 Simulation setup

In our simulation setup, we followed the experimental protocol from C-LAMP (Randerson et al., 2009) to facilitate comparison with other terrestrial biogeochemistry models. JeDi-DGVM was run with 2000 randomly-sampled plant growth strategies on a global grid at a spatial resolution of approximately 2.8° × 2.8° resolution, covering all land areas except Antarctica. The model was forced at a daily time step with downward shortwave and longwave radiation, precipitation, and near-surface air temperature from an improved NCEP/NCAR atmospheric reanalysis dataset (Qian et al., 2006). We looped the first 25 yr of the reanalysis dataset (1948–1972) with a fixed, preindustrial atmospheric

CO_2 concentration until the vegetation and soil carbon pools reached a quasi-steady state (~ 3500 yr). After this spinup simulation, a transient simulation was run for years 1798–2004 using prescribed global atmospheric CO_2 concentrations from the C4MIP reconstruction of Friedlingstein et al. (2006). This transient simulation was forced by the same climate forcing as the spinup run for years 1798–1947 and by the full reanalysis dataset for years 1948–2004. We ran an additional experiment to compare the response of JeDi-DGVM to a sudden increase in atmospheric CO_2 with results from the Free-Air CO_2 Enrichment (FACE) experiments (Norby et al., 2005). This FACE experiment simulation was similar to the transient simulation described above but with the atmospheric CO_2 concentration set to 550 ppm for years 1997–2004. We deviated from the C-LAMP experimental protocol by allowing the vegetation to evolve dynamically through the simulations, rather than prescribing the pre-industrial land cover dataset. The aspects of the C-LAMP protocol related to N deposition were not considered as a nitrogen cycle has not yet been implemented in JeDi-DGVM.

3.2 Evaluation protocol

We evaluated the performance of the JeDi-DGVM against multiple observational datasets using a set of systematic metrics developed for the C-LAMP (Randerson et al., 2009). As computed, each C-LAMP metric falls somewhere between zero and one and is then scaled by a numerical weight to produce a score. The weights are based on subjective estimates of a metric's uncertainty, considering both the measurement precision of the observations and the scaling mismatch between the model and observations. Further details about each metric and the justifications behind their particular numerical weighting are described in Randerson et al. (2009). The metrics, their weights, along with the resulting scores for JeDi-DGVM are summarized in Table 1. The scores for two terrestrial biogeochemistry models based on the PFT concept, CLM-CN (Thornton et al., 2007) and CLM-CASA' (Fung et al., 2005; Doney et al., 2006), are also shown for comparison (both were previously evaluated in Randerson et al., 2009).

Below, we provide a brief summary of the datasets and scoring methods. The results of the evaluation are described in the following section.

3.2.1 Phenology

We compared the simulated leaf area index (LAI) values against observations from the
MODerate resolution Imaging Spectroradiometer (MODIS) (Myneni et al., 2002; Zhao et al., 2005; MOD15A2 Collection 4). We consider three phenology metrics, the timing of maximum LAI, the maximum monthly LAI, and the annual mean LAI. All three metrics used monthly mean LAI observations and modelled estimates from years 2000 to 2004. The LAI phase metric was computed at each grid cell as the offset in months
between the observed and simulated maximum LAI values, normalized by the maximum possible offset (6 months), and finally, averaged across biomes. The maximum and annual mean LAI metrics M were computed using the equation:

$$M = 1 - \frac{\sum\limits_{i=1}^{n} \frac{|m_i - o_i|}{m_i + o_i}}{n} \qquad (1)$$

where m_i is the simulated LAI at the grid cell corresponding to the satellite observation
(o_i) and n is the number of model grid cells in each biome. Global means for these metrics were computed by averaging M across different biome types.

3.2.2 Global patterns of productivity and evapotranspiration

Modelled estimates of net primary productivity (NPP) are compared against a compilation of field-based observations from the Ecosystem Model Data Intercomparison
(EMDI) (Olson et al., 2001) and remote sensing-based estimates extracted from the MODIS MOD17A3 Collection 4.5 product (Heinsch et al., 2006; Zhao et al., 2005, 2006). We compared the mean annual NPP as simulated by JeDi-DGVM for years 1975–2000 with the EMDI observations on a point-by-point basis of each observation

Title Page

Abstract | Introduction

Conclusions | References

Tables | Figures

◄ | ►

◄ | ►

Back | Close

Full Screen / Esc

Printer-friendly Version

Interactive Discussion

site to the corresponding model grid cell using Eq. (1) described above. As a second NPP metric, we used Eq. (1) again with the modeled and observed values averaged into discrete precipitation bins of $400\,\mathrm{mm\,yr^{-1}}$. For the third and fourth NPP metrics, we computed the square of the Pearson coefficient of determination (r^2) between the mean annual MODIS and modelled NPP (for years 2000–2004) for all non-glaciated land grid cells and for the zonal means.

In addition to the NPP metrics from the C-LAMP protocol, we also evaluated JeDi-DGVM against spatially-explicit, data-driven estimates of evapotranspiration (ET; Jung et al., 2010) and gross primary productivity (GPP; Beer et al., 2010). The estimate of ET (Jung et al., 2010) was compiled by upscaling FLUXNET site measurements with geospatial information from remote sensing and surface meteorological data using a model tree ensemble algorithm (Jung et al., 2009). It covers years 1982–2008, although here, we use only use model years 1982–2004 for the comparison due to the limitation of the meteorological forcing dataset. The estimate of GPP (Beer et al., 2010) was derived from five empirical models calibrated also against FLUXNET observations. It covers years 1998–2005, although here, we use only use model years 1998–2004 for the comparison.

3.2.3 Seasonal cycle of atmospheric CO_2

We simulated the annual cycle of atmospheric CO_2 by applying the atmospheric impulse response functions from the Atmospheric Tracer Transport Model Intercomparison Project (TRANSCOM) Phase 3 Level 2 experiments (Gurney et al., 2004) to the JeDi-DGVM net ecosystem exchange (NEE) fluxes. The monthly JeDi-DGVM NEE fluxes for years 1991–2000 were aggregated into the 11 TRANSCOM land basis regions. The aggregated NEE fluxes are multiplied by monthly response functions from Baker et al. (2006), yielding simulated atmospheric CO_2 time series for 57 observation stations around the globe. This process was repeated for all 13 TRANSCOM atmospheric transport models and the multi-model mean annual cycle was compared with observations from the GLOBALVIEW dataset (Masarie and Tans, 1995). We computed

Jena Diversity DGVM

R. Pavlick et al.

the square of the Pearson correlation coefficient (r^2) as a measure of phase and the ratio of modeled amplitude A_M to observed amplitude A_O as a measure of magnitude (see Eq. 2).

$$M = 1 - \left| \frac{A_M}{A_O} - 1 \right| \tag{2}$$

These two metrics were computed for three latitude bands in the Northern Hemisphere (EQ–30° N, 30–60° N, 60–90° N). All stations within each band were weighted equally. The scores from the mid and high latitude bands were given more weight due to the stronger annual signal and the relatively smaller contributions from oceanic and anthropogenic fluxes.

3.2.4 Interannual variability in CO_2 fluxes

The same TRANSCOM response functions (Baker et al., 2006) and the GLOBALVIEW CO_2 measurements (Masarie and Tans, 1995) described above were combined to obtain estimates of the interannual variability in the global terrestrial NEE fluxes for years 1988–2004. We compared these estimates with JeDi-DGVM, again incorporating information about the phase and magnitude. The phase agreement was evaluated by the coefficient of determination (r^2) between the simulated global annual mean NEE fluxes and the TRANSCOM-based estimates. The magnitude of interannual variability was calculated using the standard deviation of the simulated and observation values as A_M and A_O in Eq. (2). The phase and magnitude metrics were then averaged together with equal weighting.

In their C-LAMP evaluation, Randerson et al. (2009) also evaluated the magnitude and pattern of simulated fire emissions against observations in the Global Fire Emissions Database version 2 (GFEDv2; van der Werf et al., 2006). We set the score for this metric to zero because JeDi-DGVM does not simulate fire emissions.

3.2.5 Eddy covariance measurements of energy and carbon

We compared the simulated monthly mean surface energy and carbon fluxes against gap-filled L4 Ameriflux data (Falge et al., 2002; Heinsch et al., 2006; Stoeckli et al., 2008). For each Ameriflux data-month, we sampled the corresponding model grid out-
put. Then, we constructed an annual cycle of monthly means and using Eq. (1) computed metrics for NEE, GPP, and the fluxes of sensible and latent heat. All 74 tower sites were weighted equally.

3.2.6 Carbon stocks and flows in Amazonia

We evaluated the simulated aboveground living biomass in Amazonia against the LBA-
ECO LC-15 Amazon Basin Aboveground Live Biomass Distribution Map compiled by Saatchi et al. (2007). We used Eq. (1) to calculate the model-data agreement between the simulated aboveground live biomass and the observed biomass values at each grid cell within the Amazon Basin. The model output used for comparison was the sum of the simulated aboveground wood and leaf carbon pools for year 2000. Although, not
part of the metric calculation, we also compared the model results with carbon budget observations from three mature forest ecosystems in Amazonia (Malhi et al., 2009).

3.2.7 Sensitivity of NPP to elevated CO_2 concentrations

To evaluate the sensitivity of simulated NPP to elevated CO_2 concentrations, we performed a model experiment (described above in Sect. 3.1) to mimic the treatment plots
in FACE experiments. We calculated the mean percentage increase in NPP between the control and elevated CO_2 simulations for years 1997–2001. Using Eq. (1), we compared the simulated increases at four temperate forest grid cells with corresponding site-level average increases reported by Norby et al. (2005). We also report a global map of the simulated NPP response to a step change in CO_2 concentrations from
ambient to 550 ppm.

4 Results

The Jena Diversity DGVM described in this paper presents a new approach to terrestrial biogeochemical modeling, in which the functional properties of the vegetation emerge as a result of reproductive success and productivity in a given climate. This
5 contrasts with the standard approach to mechanistic land surface modeling that utilizes a set of fixed PFTs, whose pre-determined properties are specified by parameter values often determined from databases of observed plant trait values. In an effort to understand if a more diverse representation of the terrestrial biosphere can reasonably capture observed patterns of biophysical and biogeochemical states and fluxes, we
10 contrast below the performance of the less constrained JeDi-DGVM approach against the performance of two previously evaluated land surface models.

4.1 Biodiversity patterns

In contrast to standard DGVMs, the broad sampling across a multi-dimensional trait space allows JeDi-DGVM to provide insight into potential plant biodiversity through an
15 examination of the simulated functional richness (the number of sampled plants that survive in a grid cell). The geographic pattern of simulated functional richness (Fig. 2a) is highly and significantly ($r^2 = 0.71$) correlated with a map of vascular plant species richness derived from observations (Kreft and Jetz, 2007). Out of the 2000 randomly-assembled plant growth strategies, 1411 growth strategies survived in at least one grid
20 cell and the maximum value for a single grid cell was 1322 in Western Amazonia. These fractions of surviving growth strategies are much higher than those reported by KM2000. This is likely attributable to the difference in the survival criterion. In the earlier model of KM2000, the criteria for survival was whether or not a growth strategy was able to produce more seed carbon over its lifetime than its initial amount of seed
25 carbon. Here, the criterion for survival was simply whether or not a growth strategy was able to maintain a positive carbon balance. Nonetheless, JeDi-DGVM is still able to reproduce the observed broad global pattern of plant diversity through mechanistic

environmental filtering due to functional trade-offs, and without invoking historical, competitive, or other factors.

The mean relative abundance distributions for four richness classes (Fig. 3a) are similar in shape to left-skewed log-normal distributions commonly observed through-
5   out nature (McGill et al., 2007). The left skewness means that rare species are greater in number than abundant ones, another commonly observed attribute, especially in tropical rainforests (Hubbell, 1997). With increasing levels of functional richness, the mean as well as the variance of the relative abundance distribution successively shifts to lower values. We also see that there is not necessarily one optimal combination of
10 trait parameters for obtaining high biomass in an environment, but often many differing growth strategies can reach similarly high levels of fitness (cf. Marks and Lechowicz, 2006; Marks, 2007). As the climate becomes less constraining, in terms of increasing availability of light and precipitation, the range of feasible plant growth strategies increases. The ranked abundances of growth strategies (Fig. 3b) clearly show that the
15 simulated relative abundances become increasingly even with higher richness. This pattern is also evident when visually comparing the maps of simulated function richness (Fig. 2a) and community evenness (Fig. 2b). This simulated trend towards greater evenness in more productive regions qualitatively reproduces the observed trend in rank-abundance plots of forests that show a much steeper decline in abundance in
20 boreal forests than in tropical rainforests (Hubbell, 1979, 1997).

4.2   Phenology

For the C-LAMP phase metric, JeDi-DGVM received a score of 5.0 out of 6, performing comparably with the two other land surface models (CLM-CN and CLM-CASA') previously evaluated in Randerson et al. (2009). Figure 4 shows the comparison between
25 the simulated and observed month of maximum LAI. The simulated timing of peak LAI matched observations reasonably well in the moisture-limited grassland and savannah regions of South America, Africa, and Australia. There were two clear patterns of bias, however. First, like CLM-CN and CLM-CASA', JeDi-DGVM simulated maximum

LAI occuring about one month later than the MODIS observations across much of the Northern Hemisphere. Second, in the MODIS dataset, leaf area follows the seasonality of incident solar radiation across large parts of the Amazon Basin, peaking during the early to mid part of the dry season when radiation levels are high and deep-rooted
5 vegetation still has access to sufficient moisture (Myneni et al., 2007). JeDi-DGVM did not capture this opportunistic behavior, simulated peak LAI in the tropical moist forests of Amazonia, Central Africa, and Southeast Asia occurs during the rainy season. However, the issue of whether or not tropical forests green-up during dry periods is still not settled (Samanta et al., 2010; Asner and Alencar, 2010).
10 The comparisons of simulated and observed maximum and mean LAI are shown in Figs. 5 and 6. Overall, JeDi-DGVM matched the observed values reasonably well, receiving scores of 3.7/4.0 (score/maximum score) and 4.7/5.0 for the mean and maximum LAI metrics, on par with the performances of CLM-CN and CLM-CASA'. The simulated mean LAI values were generally low relative to the observations across the
15 boreal forest region. Also, both the simulated mean and maximum LAI were higher than observed values in several regions, particularly southeast Brazil, Northeast India, the Central United States, much of Europe, and Eastern China. This may simply be due to the fact that human land-use was not accounted for in the simulation set up and these regions are used extensively for agricultural purposes. These disparities could likewise
20 indicate a need for reevaluation of the trade-off costs associated with root water uptake, i.e. the construction and maintenance costs of coarse and fine roots.

Overall, the performance of JeDi-DGVM in capturing observed global phenological patterns shows great promise in using less constrained approaches that allow the dynamics of the land surface to emerge from climatic constraints.

25 **4.3 Global carbon stocks**

JeDi-DGVM simulated global stocks of vegetation, soil, and litter carbon of 637 PgC, 1904 PgC, and 208 PgC, respectively. These values are averages over the simulation period 1980–2004. The vegetation carbon stock simulated by JeDi-DGVM falls within

the range of reported values from several PFT-based DGVM studies (500–950 PgC; Cramer et al., 2001; Sitch et al., 2003; Krinner et al., 2005; Zaehle et al., 2010) and estimates from global carbon inventories (385–650 PgC; Houghton et al., 2009). Likewise, the modelled estimate for litter carbon is close to the estimate based on carbon

5 inventories (300 PgC) reported in Houghton et al. (2009). The simulated soil carbon stock also falls within previous inventory-based estimates (1200–3000 PgC; Houghton et al., 2009).

4.4 Gross Primary Productivity

JeDi-DGVM simulated a mean global terrestrial GPP of 138 PgC yr^{-1}, which is higher
10 than the data-driven estimate of 123 ± 8 PgC yr^{-1} from Beer et al. (2010), but within the range of uncertainty (118 ± 26 PgC yr^{-1}) of a recent estimate from a processed-based model forced with remote sensing observations (Ryu et al., 2011). The zonally-averaged simulated GPP shows close agreement ($r^2 = 0.89$) with the median estimate from Beer et al. (2010), falling within or near the range of uncertainty across most
15 latitudes (Fig. 7a). JeDi-DGVM performed comparably with five PFT-based biosphere models evaluated in that study in reproducing the latitudinal pattern of GPP. Averaging zonally hides some offsetting regional biases, however. For instance, simulated productivity in Amazonia is about 25 % lower than observation-based estimates, but productivity is overestimated throughout most of the Asian tropics (Fig. 8). Overall though,
20 the broad spatial pattern of GPP is reasonably well captured by JeDi-DGVM ($r^2 = 0.85$) when compared to the map of data-driven estimates from Beer et al. (2010).

4.5 Net Primary Productivity

JeDi-DGVM simulated a mean global terrestrial NPP of 79 PgC yr^{-1}, which is more than one standard deviation greater than the mean estimate from a recent meta-analysis of
25 global NPP studies (56 ± 14 PgC yr^{-1}; Ito, 2011). We hypothesize that this overestimation stems, in part, from the lack of nitrogen limitation within the model. Global analyses

of nutrient limitation studies (Elser et al., 2007; LeBauer and Treseder, 2008) suggest that soil nitrogen availability and the energetic cost of nitrogen fixation and active ion uptake limit terrestrial productivity by about 20 %. Adding a mechanistic representation of plant nitrogen acquisition based on plant energetic trade-offs (e.g. J. Fisher et al., 2010) to future versions of JeDi-DGVM is critical, as it is thought that nitrogen availability will likely constrain the capacity of terrestrial ecosystems to continue taking up a large part of anthropogenic carbon emissions (Reich et al., 2006).

In a site-by-site comparison with field-based EMDI NPP observations (Fig. 9), JeDi-DGVM performed on par with CLM-CN and CLM-CASA' with a score of 1.5/2.0. JeDi-DGVM does relatively well in capturing the variability in NPP across the EMDI observation network (Fig. 9a), although it tends to overestimate NPP, particularly at intermediately productive sites. JeDi-DGVM also performed reasonably well and comparably with the PFT-based models when the simulated NPP is binned by precipitation class (Fig. 9b). JeDi-DGVM underestimated NPP at the driest sites ($< 400\,mm\,yr^{-1}$) and overestimated NPP at wetter sites.

For the two MODIS NPP metrics, JeDi-DGVM performed on par with CLM-CN and CLM-CASA', receiving scores of 1.6/2.0 (spatial pattern) and 1.9/2.0 (zonal means). The comparison with the MODIS NPP product reveals that JeDi-DGVM is able to capture the broad spatial patterns of NPP (Fig. 10). JeDi-DGVM prominently overestimates productivity, though, in the grassland regions of South America and the Sahel as well as the forested regions of the Eastern United States, Eastern China, and Northern Eurasian. This high bias also emerges in the comparison with the zonally averaged MODIS NPP (Fig. 7b).

4.6 Evapotranspiration

JeDi-DGVM simulated a mean global terrestrial ET flux of $82 \cdot 10^3\,km^3\,yr^{-1}$, which is higher than the observation-based estimate of $65 \pm 3 \cdot 10^3\,km^3\,yr^{-1}$ of Jung et al. (2010) but within the range of model-based estimates ($60\text{--}85 \cdot 10^3\,km^3\,yr^{-1}$) from the the Water Model Intercomparison Project (WaterMIP; Haddeland et al., 2011). Figure 11 shows

Jena Diversity DGVM

R. Pavlick et al.

a spatial comparison of simulated mean annual ET and the observation-based estimates of Jung et al. (2010). Overall, the model performed reasonably well ($r^2 = 0.78$) in reproducing the global pattern of ET. The zonal averages, however, show a strong positive bias in the equatorial tropics (Fig. 7c; $r^2 = 0.80$). Further analysis revealed that some of this model bias is attributable to an overestimation of canopy interception, especially in tropical forests. Adjusting the parameterizations related to canopy interception and canopy storage capacity has improved model performance for other DGVMs (Bonan and Levis, 2006; Liang and Xie, 2008).

4.7 Seasonal cycle of atmospheric CO_2

JeDi-DGVM captured the general temporal pattern ($r = 0.84 \pm 0.04$, 0.83 ± 0.08, 0.80 ± 0.15) of a spring drawdown of atmospheric CO_2 in the Northern Hemisphere followed by an autumnal rise. However, there is a phase offset at many stations with the simulated spring drawdown occurring about one to two months later than observations. This offset may be due to the late leaf expansion mentioned above (Fig. 4) or to limitations stemming from the simple nature of heterotrophic respiration scheme. JeDi-DGVM overestimated the seasonal amplitude of atmospheric CO_2 in the Northern Hemisphere, particularly in the middle and high latitude bands. The ratios of simulated to observed amplitudes were 1.23 ± 0.08, 1.33 ± 0.26, and 1.10 ± 0.16, for the high, middle, and equatorial latitude bands, respectively. This overestimation in seasonal amplitude is directly attributable to the overestimation of NPP in those regions. Figure 12 illustrates the reasonably good agreement between the simulated seasonal CO_2 cycle and GLOBALVIEW measurements at a high latitude (Point Barrow, Alaska, United States), a mid-latitude (Niwot Ridge, Colorado, United States), and an equatorial station (Mauna Loa, Hawaii, United States). The results for all GLOBALVIEW stations considered here are summarized in a Taylor diagram (Taylor, 2001) in Fig. 13.

Overall, JeDi-DGVM performed better than CLM-CN and CLM-CASA' on this metric with a combined score of 11.8/15.0. It scored better than both PFT-based models on

Title Page

Abstract | Introduction

Conclusions | References

Tables | Figures

◄ | ►

◄ | ►

Back | Close

Full Screen / Esc

Printer-friendly Version

Interactive Discussion

the measure of amplitude agreement and fell between the scores of those models on the measure of phase agreement.

4.8 Net terrestrial carbon exchange

The net terrestrial carbon sink simulated by JeDi-DGVM is compatible with decadal budgets of the global carbon cycle given the uncertainties regarding the oceanic and anthropogenic fluxes. For the 1980s, JeDi-DGVM simulated a global terrestrial carbon flux of $-2.89\,\mathrm{PgC\,yr^{-1}}$ (negative values indicate a net uptake of carbon by the terrestrial biosphere), which lies within the range of uncertainty from the IPCC (-3.8 to $0.3\,\mathrm{PgC\,yr^{-1}}$; Denman et al., 2007). In agreement with the IPCC carbon budgets, JeDi-DGVM simulated a larger carbon sink in the 1990s ($-3.35\,\mathrm{PgC\,yr^{-1}}$), which also lies within the IPCC range of -4.3 to $-1.0\,\mathrm{PgC\,yr^{-1}}$ (Denman et al., 2007). The model estimates presented here suggest a stronger land carbon sink than previous DGVM studies (1.2–2.75 PgC; Sitch et al., 2008; Randerson et al., 2009).

JeDi-DGVM captured the magnitude of interannual variability of terrestrial NEE quite well ($\sigma = 0.94\,\mathrm{PgC\,yr^{-1}}$) when compared to the TRANSCOM-derived estimates ($\sigma = 1.04\,\mathrm{PgC\,yr^{-1}}$) or the period 1988–2004. The model results are also moderately correlated ($r = 0.42$; $p < 0.05$) with the year-to-year TRANSCOM anomalies. The simulated anomalies fell within one standard deviation of the multi-model TRANSCOM mean in 12 of the 17 yr.

The model captured the strong positive anomaly associated with the 1998 El Niño event, but not the similarly strong anomaly in 1997. The rapid growth rate of atmospheric CO_2 in 1997 has been linked with large peat and forest fires in the Asian tropics (Page et al., 2002; van der Werf et al., 2008). Incorporating mechanistic representations of fire (e.g. Thonicke et al., 2008) and peat dynamics (e.g. Kleinen et al., 2011) in JeDi-DGVM may improve performance on this metric.

JeDi-DGVM was also not able to capture the negative anomaly in 1992–1993. This drawdown has been associated with climate impacts from the Mount Pinatubo eruption, including an increase in diffuse radiation due to elevated stratospheric aerosol loads

(Gu et al., 2003; Mercado et al., 2009). A more detailed canopy radiation transfer model (e.g. Drewry et al., 2010) would be required to to appropriately capture the effects of diffuse light on vegetation productivity. If the two yr strongly affected by the Pinatubo eruption (1992–1993) are excluded, the model time series is highly correlated (r = 0.63; $p < 0.01$) with the interannual TRANSCOM anomalies.

4.9 Comparison with eddy covariance measurements

In the comparison with the Ameriflux observations, JeDi-DGVM performed comparably to CLM-CASA' and CLM-CN, both in terms of metric scores and overall patterns of bias. Seasonal variation in NEE was often lower in the JeDi-DGVM results than in the flux tower observations. And, although not always present, many sites showed a phase offset of one to two months delay. This is consistent with the model biases described above for the seasonal CO_2 cycle and phenology. At many of the temperate forest sites, JeDi-DGVM overestimated the length of the growing season (i.e. GPP was higher than observed in the spring and autumn) and underestimated GPP during the summer peak. Like CLM-CASA' and CLM-CN, JeDi-DGVM captured the seasonal pattern of latent heat fluxes (subscore 6.6/9.0) more accurately than that of sensible heat (5.6/9.0). JeDi-DGVM significantly overestimated the sensible heat fluxes at many sites, indicating the need for a more sophisticated treatment of canopy energy balance (e.g. Drewry et al., 2010).

4.10 Carbon stocks and flows in Amazonia

JeDi-DGVM performed reasonably well in matching the spatial pattern of aboveground living biomass density in South America (Fig. 15, r = 0.83). Within the Amazon Basin, JeDi-DGVM simulated a total aboveground biomass of 59 PgC, slightly lower than the total of 69 ± 7 PgC estimated from observations by Saatchi et al. (2007). We attribute some of the overestimation of biomass around the perimeter of the Amazon Basin and further south in the Paraná basin to a lack of human land-use and fire as

model processes/drivers. The underestimation of aboveground biomass in the Central Amazon Basin may be related to the lack of competitive interactions between plant growth strategies. More specifically the competition for light, which if incorporated in the model might favor plant growth strategies that invest proportionally more carbon towards growing woody stems. The implications of the current "biomass-ratio" aggregation scheme and the current lack of resource competition within JeDi-DGVM are discussed further in Sect. 5.3.

The carbon allocation and storage scheme in JeDi-DGVM provides a basis for contrasting model estimates of carbon pools against carbon budget observations from three mature forest ecosystems in Amazonia synthesized by Malhi et al. (2009). This comparison is summarized in Fig. 16. Despite differences between GPP simulated by JeDi-DGVM ($2474\,\mathrm{gC\,m^{-2}\,yr^{-1}}$) and observed values ($3330 \pm 420\,\mathrm{gC\,m^{-2}\,yr^{-1}}$; Figueira et al., 2008; Malhi et al., 2009), we find that JeDi-DGVM performs well when contrasting Amazon carbon pool and allocation flux estimates. The simulated ratio of autotrophic respiration to GPP (52 %) was slightly less than the range of the observations (65 ± 10 %). The fractions of NPP allocated to each plant carbon pool correspond quite well with the observed allocation patterns. The simulated turnover times for the woody pools (37 yr) closely matches the the mean of the observations ($40 \pm 4\,\mathrm{yr}$) from Malhi et al. (2009). Other studies, however, have suggested much longer wood turnover times ($\sim 90\,\mathrm{yr}$) (Vieira et al., 2004; Figueira et al., 2008). The simulated stock of coarse woody debris ($2421\,\mathrm{gC\,m^{-2}}$) closely matches the range of observed values ($2421 \pm 560\,\mathrm{gC\,m^{-2}}$). The mean simulated soil carbon stock ($23\,460\,\mathrm{gC\,m^{-2}}$) for this region is significantly greater than the mean of the observations to 2 m depth ($14\,260 \pm 2728\,\mathrm{gC\,m^{-2}}$; Malhi et al., 2009). However, Quesada et al. (2009) presents evidence for substantial carbon storage below that depth, including a soil carbon stock of $22\,000\,\mathrm{gC\,m^{-2}}$ to 3 m depth at the Tapajós site.

4.11 Sensitivity to elevated atmospheric CO_2

Globally, simulated NPP increased by 18 % during the first five yr of simulated CO_2 enrichment at 550 ppm, exhibiting a large step change in the first yr. Not surprisingly, simulated net terrestrial carbon uptake also quickly rose to 15.03 PgC yr^{-1} during that time.
5 These values are similar to those exhibited by CLM-CASA' (17 % and 12.5 PgC yr^{-1}).
During the same time period (1997–2001), mean NPP increased by 15 ± 1 % at the model grid cells corresponding to the four temperate forest FACE experiments reported in Norby et al. (2005). The observed increase at those sites was higher, 27 ± 2 %. The geographic variation of NPP enhancement (Fig. 17) is broadly similar to the pattern
10 simulated by the global vegetation model LPJ-GUESS (Hickler et al., 2008), with the strongest enhancement occurring in tropical forest regions. JeDi-DGVM performed reasonably well on this metric with a score of 6.9/10. This was close to the performance of CLM-CASA' and significantly better than CLM-CN.

4.12 Summary of evaluation

15 Overall, JeDi-DGVM received a score of 68.2 (out of 100 possible), exceeding the scores of the two PFT-based models (CLM-CASA'; 65.7 and CLM-CN; 58.4) evaluated in Randerson et al. (2009). The scores of the individual metrics are summarized in Table 1. JeDi-DGVM matched or exceeded the performance of at least one of the other models on almost every metric. The two exceptions were the comparisons with
20 estimates of interannual terrestrial carbon exchange and fire emissions.

The results of this evaluation imply that that the bottom-up functional trade-off approach of JeDi-DGVM, linked with an aggregation mechanism based on the "biomass-ratio" hypothesis, is capable of simulating the broad-scale patterns of terrestrial biogeochemistry at least as well as two other state-of-the-art terrestrial biosphere models
25 based on the dominant PFT paradigm. We have also shown that unlike PFT-based DGVMs, JeDi-DGVM is able to mechanistically represent the large-scale biogeographical patterns of plant species richness, community evenness, and relative abundance

distributions, opening avenues to explore the impacts of future climate variability on terrestrial ecosystem composition and function in a much less constrained way than has been previously performed.

5 Discussion

JeDi-DGVM introduces several elements novel to dynamic vegetation modeling, allowing for an explicit representation of functional diversity that can evolve temporally. As the current implementation represents an initial prototype from which refinements and added functionality will be made, we discuss below several key concepts that underlie the formulation of JeDi-DGVM, and which will likely result in the greatest impact on model improvement in future efforts.

5.1 Representation of trade-offs

JeDi-DGVM is a prototype meant to explore the potential utility of a trait-based functional trade-off approach for transitioning the state-of-the-art of global vegetation modelling beyond the limitations of a set of fixed PFTs. One of the greatest potential advantages of this approach is that it does not constrain the vegetated land surface to be represented by a small set of functional types, but instead allows for a more continuous representation of vegetation types that can evolve as a function of climatic suitability. We demonstrate in this work that from this trade-off-based approach a realistic representation of land surface biophysical form and function can emerge.

For this approach to be successful, several key requirements must be met, particularly (1) identification of the key trade-offs that determine the ability of a plant to survive in a given environment, and (2) proper parameterization of the costs and benefits of the traits associated with those trade-offs. In this current implementation, JeDi-DGVM utilizes 15 functional parameters that characterize the behavior of a growth strategy in terms of its carbon allocation strategy, phenological dynamics, tissue turnover and the

balance between respiration and photosynthesis. The positive performance of JeDi-DGVM in the C-LAMP evaluation lends credibility to this approach, and will motivate further evaluation of the critical plant traits and trade-offs that determine the performance of the vegetated land surface. New information sources linking costs and benefits with observed traits, such as the TRY database (Kattge et al., 2011), will provide important constraints on future refinements of this approach.

5.2 Is everything everywhere?

JeDi-DGVM assumes that the distribution of plant growth strategies is able to adjust quickly to climatic changes, allowing all of the sampled plant growth strategies to emerge when a given climate anywhere on the globe becomes suitable. This can be stated through the ecological hypothesis of "Everything is everywhere, but the environment selects." While this ecological hypothesis was originally formulated with respect to the biogeography of marine microbes, terrestrial plant species face considerable barriers to migration (e.g. mountain ranges, deserts, oceans). The timescales of terrestrial plant growth and dispersal also differ greatly from those of fast-lived marine microbes transported along ocean currents. A model-based study (Malcolm et al., 2002) showed that the preferred ranges of many plant species could shift tens to hundreds of kilometers over the next century due to anthropogenic greenhouse warming, making the issue of estimating migration rates, and the extent to which everything is truly everywhere, key to predicting future vegetation composition.

Despite the importance of this issue to the vegetation modelling community (Neilson et al., 2005), only one modelling group (Lee, 2011) has introduced mechanistic migration processes in a DGVM. Lee (2011) attributes this partially to the difficulties associated with the considerable variation in seed dispersal rates within the PFTs used by the current generation of DGVMs. Incorporating aspects of seed dispersal in a functional trade-off framework, through additional traits such as seed size, could help to constrain plant migration rates in climate change simulation experiments. Seed dispersal range, and consequently the rate of plant migration, is closely linked to seed size. Smaller

seeds are more easily transported by the wind and animals than larger seeds (Ezoe, 1998). On the other hand, larger seeds allow establishing plants to persist through longer periods of stress. Parameterizing the trade-off between seed size and dispersal rates will be challenging but possibly less so than modelling migration with a PFT-based

5 scheme.

5.3 Aggregation scheme and competition

The aggregation of vegetation states and fluxes across the diversity represented in each computational grid cell is based on the "biomass-ratio" hypothesis. This scheme determines the grid cell flux or state as an average across all surviving plant growth

10 strategies in the grid cell, weighted by their respective biomass, imposing the implicit assumption that interaction between plant growth strategies is weak. For example, JeDi-DGVM does not currently account for shading of plant growth strategies that resemble understory plants by those that resemble dominant canopy trees. Likewise, the hydrologic conditions that a plant growth strategy experiences are not influenced

15 by the other surviving plant growth strategies in its grid cell. Thus, understory plant growth strategies do not stand to benefit during periods of drought from the observed phenomena of hydraulic distribution, wherein deep-rooted plants redistribute soil water from lower soil layers (Lee et al., 2005; Prieto et al., 2012). These types of competitive and facilitative interactions are known to influence community-assembly processes at

20 the local scale (Cavender-Bares et al., 2009), leading to trait divergence. However, at larger scales, including the spatial resolution of the simulation results presented here, trait selection and trait convergence due to environmental filtering have been shown to be the dominant community-assembly processes (Kraft et al., 2008; Swenson and Weiser, 2010; Freschet et al., 2011; Kraft et al., 2011).

25 This "biomass-ratio" aggregation scheme was chosen for its simplicity and its demonstrated effectiveness for making statistical predictions about community fluxes from trait abundance information at the field-scale (Garnier et al., 2004; Vile et al., 2006; Kazakou et al., 2006; Díaz et al., 2007; Quetier et al., 2007). However, the

mechanistic trade-off-based trait filtering framework of JeDi-DGVM does not preclude the integration of more sophisticated aggregation schemes. For example, Bohn et al. (2011) recently used JeDi-DGVM model output together with a simple population dynamics model DIVE (Dynamics and Interactions of VEgetation) to explore how seed
5 competition, resource competition and environmental disturbance might influence community structure. In the future, the trade-off-based modelling approach of the JeDi-DGVM could be directly integrated with the representation of population dynamics from the DIVE model or from other recent models (e.g. the Ecosystem Demography model; Moorcroft et al., 2001; Medvigy et al., 2009; R. Fisher et al., 2010) which explicitly
10 account for canopy height structure and age classes.

5.4 Further evaluation

Here, we evaluated the feasibility of using the JeDi-DGVM modelling approach to simulate broad-scale patterns of terrestrial biogeochemistry and ecosystem properties. However, another key and unique test for this approach would be to directly compare
15 the emergent patterns of simulated FT parameters with our growing knowledge about the geographic distribution of plant traits and their environmental co-variates. This information could come from trait databases (e.g. TRY; Kattge et al., 2011) or remote sensing products (e.g. canopy nitrogen observations; Ollinger et al., 2008). A further test would be to compare simulated shifts in FT parameters and allocation patterns with
20 observed shifts in trait abundances from ecosystem manipulation experiments, e.g. irrigation (Axelsson and Axelsson, 1986), CO_2 enhancement (Ainsworth and Long, 2004), or throughfall exclusion (Fisher et al., 2007). These fine-scale comparisons would help further refine various aspects of the biogeochemical formulations and trade-offs incorporated into JeDi-DGVM, and give greater confidence in projections regarding the
25 future fate of the terrestrial biosphere.

In Sect. 4.10, we briefly compared the simulated allocation of NPP to different plant carbon pools with carbon budget observations (Malhi et al., 2009) from three Amazonian forest ecosystems. This analysis should be expanded globally by comparing the

the simulated patterns of carbon flows and stocks with observations from other existing datasets based on carbon inventories (Cannell, 1982; Litton et al., 2007; Luyssaert et al., 2007; Malhi et al., 2011). More specifically, one could look at how the simulated allocation patterns vary along environmental gradients (cf. Litton and Giardina, 2008; Cornwell and Ackerly, 2009). In this study we only examined at the community-weighted allocation fluxes. It would be equally interesting to explore how the simulated partitioning of NPP varies among surviving plant growth strategies within grid cells (cf. Ackerly and Cornwell, 2007).

For instance, Wolf et al. (2011) and Malhi et al. (2011) found evidence that the strongest allocation trade-off was not between root and shoots, as has been commonly thought, but rather more specifically between allocation to fine roots and aboveground wood. This relationship is likely mediated between sites by hydrological conditions and within sites by the competitive dynamics between faster and slower growing trees. In principle, the functional trade-off modelling approach of JeDi-DGVM should be able to capture both of these phenomena. However, it might require the introduction of further constraints related to disturbances (Bohn et al., 2011) and FT parameters related to wood economics and plant hydraulics (cf. Hickler et al., 2006; Chave et al., 2009; Falster et al., 2010)

5.5 Potential applications

The "bottom-up" functional trade-off-based modelling framework presented here represents a step forward in the development of a comprehensive and predictive representation of the terrestrial biosphere for use in Earth System Models. By mechanistically simulating the full range and continuous nature of plant functional diversity, it will be possible to explore new areas of research including:

1. JeDi-DGVM could be used to investigate the relationships between plant biodiversity and ecosystem functioning. Experimental and theoretical ecologists have debated the magnitude and direction of these relationships for decades (McCann,

2000; Loreau, 2001; Reiss et al., 2009). Results from biodiversity manipulation experiments at the field scale, however, generally agree that diversity promotes ecosystem stability. (France and Duffy, 2006; Tilman et al., 2006; Ives and Carpenter, 2007; Proulx et al., 2010). This implies that PFT-based vegetation models, by underrepresenting functional diversity, might overestimate the response of terrestrial ecosystems to climatic variability and change. With JeDi-DGVM, it is now possible to make numerical estimates about these biodiversity-ecosystem functioning relationships at the global scale and their significance for modelling the fate of the terrestrial biosphere in the twenty-first century. This could be accomplished by running a diverse JeDi-DGVM simulation with many plant growth strategies and another simulation wherein the functional diversity is artificially reduced (e.g. recreating something like PFTs by simulating only a single plant growth strategy at each grid cell characterized by the community-weighted FT parameters from the first simulation). It would be interesting to compare the temporal variability in the simulated ecosystem fluxes of both approaches, as well as the ability of the two simulated ecosystems to adapt to changing environmental forcings.

2. By coupling the JeDi-DGVM trade-off-based approach with an optimization algorithm, it is possible to seek out those functional trait combinations that maximize a particular ecosystem service. For example, Drewry et al. (2012), have used JeDi-DGVM to investigate the the optimal set of FT parameters which maximize the allocation to seed biomass under the present-day climate of each model grid cell, allowing for estimates of the upper bound of realizable yields as a function of climatic constraint.

3. Climate model projections point towards the possibility of novel climates without modern or paleo analogs (Jackson and Williams, 2004; Williams and Jackson, 2007). This causes difficulties for PFT-based modelling approaches because they often rely so heavily on bioclimatic relationships based on present-day empirical observations. Because JeDi-DGVM samples FT parameters from their full

theoretical ranges, it may produce surviving growth strategies or compositions of growth strategies without present-day analogs (Reu et al., 2012). Coupling JeDi-DGVM directly within an Earth System Model would allow for the exciting possibility of exploring how these no-analog vegetation compositions influence atmosphere-biosphere interactions.

6 Conclusions

In this paper, we introduced the JeDi-DGVM, which represents a new class of dynamic global vegetation models based on simulating the performance of many randomly-assembled hypothetical plant growth strategies, rather than the traditional approach of using a small number of PFTs defined a priori. In a systematic evaluation, we have shown that its bottom-up plant functional trade-off approach together with a simple mass-based aggregation mechanism is able to capture the broad patterns of terrestrial biogeochemical fluxes and associated land surface properties reasonably well. The evaluation results compare favorably with two other state-of-the-art terrestrial biosphere models based on the older PFT paradigm. Additionally, we have shown that JeDi-DGVM is able to mechanistically reproduce the global-scale biogeographical patterns of plant species richness and community evenness. Because it is more closely based on first-principles, JeDi-DGVM requires less input data and is able to produce a wider range of testable outputs than earlier DGVMs based on the PFT concept. This new approach sets the foundation for future applications, in which the simulated vegetation response to global change has a greater ability to adapt through changes in ecosystem composition, having potentially wide-ranging implications for biosphere-atmosphere interactions under global change.

Appendix A

Jena Diversity-Dynamic Global Vegetation (JeDi-DGVM) model description

JeDi-DGVM builds upon the plant diversity model of KM2000, which itself took many model formulations from earlier land surface (Roeckner et al., 1996) and terrestrial biosphere models (e.g. Potter et al., 1993; Knorr and Heimann, 1995; Kaduk and Heimann, 1996). Here, the ecophysiological parameterizations have been kept relatively simple to keep the computational requirements manageable. This makes it possible to simulate many the development of many plant growth strategies in parallel across a global grid over long simulation periods within a reasonable timeframe on a single Linux workstation. That said, several of the formulations and parameter values, particularly with respect to the calculation of productivity and respiration, have been changed to improve the realism of the simulated fluxes. Also, whereas the KM2000 model simulated the life-cycle of individual generic plants from germination to death, the JeDi-DGVM introduces tissue turnover and thus simulates something closer to the mean of a population for each plant growth strategy. Finally, the most important new feature is the introduction of a scaling mechanism to aggregate the exchange fluxes and land-surface properties of many plant growth strategies to the community-level based on the "biomass-ratio" hypothesis.

A1 Plant module overview

The plant module simulates the development of plant growth strategies based on the fundamental ecophysiological processes of photosynthesis, respiration, allocation, phenology, and reproduction. Plant development is coupled in a process-based manner to a land-surface hydrology module which simulates canopy interception, throughfall, infiltration, evaporation, root-water uptake, and surface runoff, using daily meteorological forcing of downwelling shortwave and net longwave radiation, precipitation, and near-surface air temperature. The variables and parameters involved in the

Title Page

Abstract | Introduction

Conclusions | References

Tables | Figures

◄◄ | ►►

◄ | ►

Back | Close

Full Screen / Esc

Printer-friendly Version

Interactive Discussion

development of the plant growth strategies are summarized in Table C1. The details of the land-surface module are described in Appendix B.

Each plant growth strategy is represented by six carbon tissue pools: stored assimilates C_A, leaves C_L, fine roots C_R, aboveground wood (branches and stems) C_{WL},
5 belowground wood (coarse roots) C_{WR}, and a reproductive (or "seed") pool C_S. When growing conditions are favorable, carbon germinates from the "seed" pool to the storage pool. The plant then begins to grow by allocating carbon from the storage pool to the various tissue pools. The tissue pools are also subject to turnover and senescence. The litter fluxes from these two processes serve as input to the soil carbon module. The
10 sizes of the tissue pools influence the parameter values of the land-surface module, affecting both the absorption of solar radiation and the land-surface hydrology. For example, the absorption of solar radiation, which supplies the energy for photosynthesis and evapotranspiration, is proportional to leaf area index (LAI) which is derived from leaf biomass. Fine root biomass affects the maximum rate of water uptake from the rooting
15 zone, influencing the plant's water status and the supply of moisture for evapotranspiration. Likewise, the coarse root biomass of a plant determines the hydrologic depth of its rooting zone. The land-surface conditions in turn affect the net primary productivity (NPP), which forms the input to the storage pool. A plant growth strategy is considered to be alive as long as the carbon in the storage pool is greater than zero ($C_A > 0$). The
20 details of these processes are described in the following subsections.

The particular functioning of a plant growth strategy is defined by a set of 15 functional trait (FT) parameters (t_1, ..., t_{15}). These FT parameters control the allocation of carbon from the storage pool to the other tissue pools, the tissue turnover rates, the phenological response to environmental conditions, and the ecophysiological balance
25 between photosynthesis and respiration. All of the FT parameters range between zero and one. However, these ranges are often extended by using the FT parameters as either exponents or coefficients. Each FT parameter is associated with one or more functional trade-offs. For instance, a higher allocation to fine roots enhances the rate at which a plant can extract moisture from the soil matrix, but this comes at the expense

of allocation to the aboveground pools and thus a decreased ability to capture light for photosynthesis, as well as the metabolic cost of maintaining that biomass. The implementation of these trade-offs are explained in further detail below. The descriptions of the FT parameters are summarized in Table C2.

A2 Vegetation carbon pool dynamics

The following differential equations describe the dynamics of the vegetation carbon pools:

$$\frac{dC_A}{dt} = \text{NPP} + \text{GERM} - \sum C_A A_{\text{tissue}}(1 - c_{\text{RES,tissue}})$$

$$\frac{dC_S}{dt} = C_A A_S (1 - c_{\text{RES,S}}) - \text{GERM} - \frac{C_S}{\tau_S}$$

$$\frac{dC_L}{dt} = C_A A_L (1 - c_{\text{RES,L}}) - \frac{C_L}{\tau_L} \tag{A1}$$

$$\frac{dC_R}{dt} = C_A A_R (1 - c_{\text{RES,R}}) - \frac{C_R}{\tau_R}$$

$$\frac{dC_{WL}}{dt} = C_A A_{WL} (1 - c_{\text{RES,WL}}) - \frac{C_{WL}}{\tau_{WL}}$$

$$\frac{dC_{WR}}{dt} = C_A A_{WR} (1 - c_{\text{RES,WR}}) - \frac{C_{WR}}{\tau_{WR}}$$

The details of the various terms are described below in the following subsections.

A3 Growing Conditions

The timing of plant growth and germination is controlled by environmental conditions, specifically, soil wetness f_W and near-surface air temperature T. Soil wetness f_W being defined as the ratio of moisture W stored in the rooting zone relative to the maximum

storage capacity of the rooting zone W_{MAX}. FT parameters t_1 and t_2 in time constants τ_W and τ_T determine how quickly a plant responds to changes in the environmental conditions.

$$f_{\text{GROW},T}(t) = \frac{T + \tau_T f_{\text{GROW},T}(t - \Delta t)}{1 + \tau_T}$$

5   with $\tau_T = 10^{4t_1 - 2}$

$$f_{\text{GROW},W}(t) = \frac{f_W + \tau_W f_{\text{GROW},W}(t - \Delta t)}{1 + \tau_W}$$

$$\text{with } f_W = \frac{W}{W_{\text{MAX}}} \quad \text{and} \quad \tau_W = 10^{4t_2 - 2} \tag{A2}$$

10    $$f_{\text{GROW},G}(t) = \frac{f_{W,\text{bare}} + \tau_W f_{\text{GROW},G}(t - \Delta t)}{1 + \tau_W}$$

$$\text{with } f_{W,\text{bare}} = \frac{W_{\text{bare}}}{W_{\text{MAX},0}}$$

Values of FT parameters t_1 and t_2 near zero represent a short memory and thus a quick response to change, while larger values represent a longer memory and a slower re-
15 sponse. For example, a plant with a low value of τ_T would react almost immediately to a warm day in early spring, whereas a plant with a larger value would react only after several days or weeks of spring warmth. Likewise, a high value of τ_W would lead a plant to continue to allocate carbon despite persisting drought conditions.

    For germination, only the soil wetness of the top 50 mm W_{top} (see Eq. B16) relative to
20 the storage capacity of bare non-vegetated soil is considered. Germination and growth only occur when both the temperature function $f_{\text{GROW},T}$ is above a critical temperature T_{crit} and the relevant soil wetness condition, $f_{\text{GROW},W}$ or $f_{\text{GROW},G}$, is greater than a critical

Printer-friendly Version

Interactive Discussion

value of 0.5. The critical temperature T_{crit} is a linear function of FT parameter t_3 between $-5\,°C$ and $10\,°C$.

$$f_{\text{GROW}} = \begin{cases} 0 & f_{\text{GROW},W} < 0.5 \quad \text{and} \quad f_{\text{GROW},T} < T_{\text{crit}} \\ 1 & f_{\text{GROW},W} \geq 0.5 \quad \text{or} \quad f_{\text{GROW},T} \geq T_{\text{crit}} \end{cases}$$

$$f_{\text{GERM}} = \begin{cases} 0 & f_{\text{GROW},G} < 0.5 \quad \text{and} \quad f_{\text{GROW},T} < T_{\text{crit}} \\ 1 & f_{\text{GROW},G} \geq 0.5 \quad \text{or} \quad f_{\text{GROW},T} \geq T_{\text{crit}} \end{cases} \tag{A3}$$

A4   Germination

Germination of carbon from the "seed" pool C_S to the storage pool C_A occurs when germination conditions are favorable ($f_{\text{GERM}} = 1$) and the "seed" pool is not empty ($C_S > 0$):

$$\text{GERM} = f_{\text{GERM}} \gamma_{\text{GERM}} \frac{C_S}{\max(p, k_{\text{GERM}})} \tag{A4}$$

with $\gamma_{\text{GERM}} = 10^{4t_4 - 4}$.

FT parameter t_4 modulates the germination fraction γ_{GERM}, the fraction of "seed" carbon C_S which can germinate to the storage pool C_A in a single daily time step (Cohen, 1968; Alvarado and Bradford, 2002). Values of t_4 near zero result in a conservative strategy with only a small fraction of "seed" carbon germinating to the storage pool per day when germination conditions are met ($f_{\text{GERM}} = 1$). Higher values yield increasingly more opportunistic strategies. When germination conditions are favorable ($f_{\text{GERM}} = 1$) and the "seed" pool is ($C_S = 0$), a small amount of initial carbon is added to the "seed" pool to allow a growth strategy to begin growth. When this occurs, an equivalent amount of carbon is added to the community-aggregated gross primary productivity (see Appendix A9) to maintain the conservation of mass in the grid-cell variables.

A5 Carbon allocation

Plants allocate carbon from the storage pool to growth when the growing conditions are favorable ($f_{GROW} = 1$). Allocation to the "seed" pool occurs when net primary productivity is greater then zero ($f_{SEED} = 1$ when NPP > 0). The amount of carbon allocated to each tissue pool is proportional to the size of the storage pool C_A and to the set of FT parameters, $t_5, \ldots, t_{10}$, which together form the plant's carbon allocation strategy:

$$
A_S = f_{SEED} \frac{t_5}{t_5 + t_6 + t_7 + t_8}
$$

$$
A_L = f_{GROW}(1 - t_9) \frac{t_6}{t_5 + t_6 + t_7 + t_8}
$$

$$
A_R = f_{GROW}(1 - t_{10}) \frac{t_7}{t_5 + t_6 + t_7 + t_8} \tag{A5}
$$

$$
A_{WL} = f_{GROW} f_{VEG} t_9 \frac{t_6}{t_5 + t_6 + t_7 + t_8}
$$

$$
A_{WR} = f_{GROW} f_{VEG} t_{10} \frac{t_7}{t_5 + t_6 + t_7 + t_8} \ .
$$

The allocation fractions are mathematically constrained such that they sum to less than one ($\sum A_{tissue} < 1$). The unallocated fraction ($1 - \sum A_{tissue}$) remains in the storage pool C_A for future growth or maintenance respiration.

A6 Turnover and senescence

The turnover times τ_{WL} and τ_{WR} of the woody tissue pools are defined as functions of FT parameter t_{11}:

$$
\tau_{WL} = \tau_{WR} = 365(79\, t_{11} + 1) \tag{A6}
$$

Eq. (A6) yields a range of turnover times between 1 and 80 yr. The base turnover time $\tau_{L,0}$ for the leaf and fine root pools is defined as a function of FT parameter t_{12}:

$$\tau_{L,0} = \frac{365}{12} 10^{2.0t_{12}} \tag{A7}$$

Eq. (A7) yields a range of turnover times log-distributed between 1 and 100 months, which covers the range of observations in the TRY database (Kattge et al., 2011). The turnover times for the "seed" and storage pools are assumed constant across all plant growth strategies (see Table C1).

Senescence is triggered when both NPP and the time-averaged net primary productivity f_{NPP} are negative, where:

$$f_{NPP}(t) = \frac{NPP + \tau_{NPP} f_{NPP}(t - \Delta t)}{1 + \tau_{NPP}} \tag{A8}$$

with $\tau_{NPP} = 10^{5t_{13}-2}$.

$$f_{SEN} = \begin{cases} 0 & f_{NPP} \geq 0 \quad \text{or} \quad NPP \geq 0 \\ 1 & f_{NPP} < 0 \quad \text{and} \quad NPP < 0 \end{cases} \tag{A9}$$

FT parameter t_{13} in time constant τ_{NPP} describes the memory to past NPP conditions. Values of t_{13} near zero represent a short persistence during periods of negative NPP, while values closer to one represent longer persistence. During periods of senescence, the turnover rates of the leaf and fine root pools increase proportional to a constant factor τ_{SEN}. The relative magnitude of this increase is determined by FT parameter t_{14}:

$$\tau_L = \left(\frac{1}{\tau_{L,0}} + \frac{1}{\tau_{SEN}} f_{SEN} t_{14} \right)^{-1}$$

$$\tau_R = \left(\frac{1}{\tau_{L,0}} + \frac{1}{\tau_{SEN}} f_{SEN} (1 - t_{14}) \right)^{-1} \tag{A10}$$

Full Screen / Esc

Printer-friendly Version

Interactive Discussion

A7 Land surface parameters

The land-surface parameters (maximum plant available water storage in the rooting zone W_{MAX}, leaf area index LAI, potential supply rate for transpiration S, fractional vegetative cover f_{VEG}, fractional forest cover f_{FOR}, snow-free surface albedo a_{ns}, and the storage capacity of the canopy W_{LMAX}) relate the development of a plant growth strategy to the coupled land-surface module which simulates its environmental conditions. The module itself is based on the land-surface component of the ECHAM4 atmospheric General Circulation Model (Roeckner et al., 1996) along with modifications introduced by KM2000 and is described in detail in Appendix B. These parameters are computed for each plant growth strategy from its carbon tissue pools and FT parameters:

$$
\begin{aligned}
\text{LAI} &= C_L \text{SLA} \\
f_{VEG} &= 1 - e^{-k\text{LAI}} \\
f_{FOR} &= 1 - e^{-c_{FOR}C_{WL}} \\
W_{LMAX} &= c_{WLMAX}\text{LAI} \\
a_{ns} &= f_{VEG}a_{VEG} + (1 - f_{VEG})a_{SOIL} \\
W_{max} &= \max\left[W_{max,0}, c_{PAW}\sqrt{c_{SRL}C_{WR}} \right] \\
S &= c_{SRU}C_R f_W
\end{aligned}
\tag{A11}
$$

The land-surface parameters and their conversion constants are summarized in Table C3.

The leaf area index LAI of a plant growth strategy is calculated as the product of its leaf biomass C_L and its specific leaf area SLA. The SLA of a plant growth strategy being estimated as a function of leaf lifespan using an empirical relationship derived by

Full Screen / Esc

Printer-friendly Version

Interactive Discussion

Reich et al. (1997), where τ_{L_0} is the base leaf turnover rate from Eq. (A7).

$$\text{SLA} = 0.030 \left(\frac{365}{\tau_{L_0}} \right)^{-0.46} \tag{A12}$$

This establishes a trade-off such that a plant growth strategy falls along a spectrum between an evergreen strategy with thicker, long-lived leaves and a deciduous strategy with thinner, short-lived leaves (Reich et al., 1998; Westoby et al., 2002; Shipley et al., 2006a).

The leaf area index LAI is then used to determine both the fractional vegetation cover f_{VEG} according to the Lambert-Beer law (Monsi and Saeki, 1953) and the water storage capacity of the canopy W_{LMAX}. The parameterization of the fractional forest cover f_{FOR} is taken as an analogy to the formulation used for vegetative cover f_{VEG}. The snow-free surface albedo a_{ns} is calculated as the mean of its canopy albedo a_{VEG} and the bare soil albedo a_{SOIL} (constant for all plant growth strategies), weighted by its fractional vegetation cover f_{VEG}. The canopy albedo a_{VEG} of a plant growth strategy is a linear function of the canopy nitrogen concentration $[N_L]$ (Hollinger et al., 2010).

$$a_{VEG} = 3.216[N_L] + 0.02 \tag{A13}$$

The formulations regarding root properties (W_{MAX} and S) are obtained from first principles. The motivation for using a square-root relationship for the maximum plant available water storage in the rooting zone comes from the Shinozaki et al. (1964) pipe model. From the pipe model perspective, the root system is viewed as an assemblage of pipes which connect the root ends (the organs responsible for water absorption from the soil) with the leaves. If we assume a uniform density of root ends within the rooting zone, we obtain a square root relationship between the depth of the rooting zone and the total length of the coarse roots (given by the product of the coarse root biomass C_{WR} and an assumed constant specific root length parameter c_{SRL}). The maximum plant available soil water storage W_{MAX} is then given by the product of this rooting zone

depth and the unit plant available water capacity c_{PAW} (i.e. the difference between field capacity and permanent wilting point per unit depth) taken from a global dataset (Dunne and Willmott, 1996). Finally, we assume the potential supply rate for transpiration S is related to the fine root biomass C_R and soil wetness f_W via a constant specific root water uptake parameter c_{SRU}.

A8 Net Primary Productivity

The net primary productivity NPP of each plant growth strategy is computed as the difference between its gross primary productivity GPP and its autotrophic respiration flux RES_a.

$$NPP = GPP - RES_a \tag{A14}$$

The parameters and variables involved in the calculation of these fluxes are summarized in Table C4.

GPP is estimated using a big-leaf non-rectangular hyperbola approach (Johnson and Thornley, 1984; Franklin, 2007):

$$GPP = \frac{h}{2\theta}\left[(\phi I_a + P_{max}) - \sqrt{(\phi I_a + P_{max})^2 - 4\theta\phi I_a P_{max}}\right]\alpha_{H_2O} \tag{A15}$$

While more sophisticated and likely more accurate photosynthesis schemes are abundant, we chose to use this relatively simple approach for its computational expediency and to keep the number of necessary parameters low. Absorbed photosynthetically active radiation I_a is derived, following the Lambert-Beer law of light extinction, from the photosynthetically active radiation (assumed to be half of downward shortwave radiation) above the canopy I_0 and the fractional coverage of vegetation (Monsi and Saeki, 1953):

$$I_a = I_0 f_{VEG} \tag{A16}$$

The light-saturated canopy photosynthetic capacity P_{max} of a plant growth strategy is estimated as a linear function of the canopy nitrogen concentration $[N_L]$ following an empirical relationship proposed by Ollinger et al. (2008) assuming a foliar carbon content of $0.48\,gC\,gDM^{-1}$. Similar relationships between N content and photosynthetic capacity are well-documented at the leaf scale (Field and Mooney, 1986; Reich et al., 1997; Wright et al., 2004).

$$P_{max} = (59.2 \cdot 10^{-4}[N_L] + 1.1 \cdot 10^{-4})\alpha_T \tag{A17}$$

$$[N_L] = 10^{t_{15}-2}$$

The canopy nitrogen concentration $[N_L]$ itself is a function of FT parameter t_{15} leading to a range of values log-distributed between 0.01 and $0.10\,gN\,gC^{-1}$. The supply of nitrogen is not considered as a limiting factor. The curvature parameter θ is assumed constant across all plant growth strategies. Daylength h is computed from the cosine of the solar zenith angle, which varies with season and latitude (Hartmann, 1994). The quantum efficiency ϕ and the factor α_T modifying the light-saturated photosynthetic capacity are computed as functions of both air temperature and ambient CO_2 concentrations following Cannell and Thornley (1998).

The moisture stress factor α_{H_2O} is a function of the the ratio between the potential supply rate for transpiration (S) and the atmospheric demand for transpiration (D; further details in Appendix B).

$$\alpha_{H_2O} = 1 - e^{-\frac{S}{D}} \tag{A18}$$

The autotrophic respiration RES_a of a plant growth strategy is calculated as the sum of its growth respiration RES_g and maintenance respiration RES_m fluxes (McCree, 1970; Thornley, 1970). Growth respiration consumes a fixed fraction $c_{RES,tissue}$ of the carbon allocated from the storage pool C_A to the each tissue pool. These fractions are assumed to be constant across all plant growth strategies.

$$RES_g = C_A \sum (A_{tissue} c_{RES,tissue}). \tag{A19}$$

Following Ryan (1991), maintenance respiration RES_m is calculated based on the nitrogen content of each tissue, a specific respiration rate $c_{RES,N}$ at 20 °C and a Q_{10} temperature function.

$$RES_m = c_{RES,N} Q_{10,a}^{\left(\frac{T-20}{10}\right)} [N_L][(C_L + C_R) + c_{sapwood}(C_{WL} + C_{WR})] \tag{A20}$$

5 The fine root nitrogen concentration $[N_R]$ is assumed to be equal to the leaf nitrogen concentration $[N_L]$ for all plant growth strategies. The fractions of sapwood carbon to woody carbon (0.05) and sapwood nitrogen to leaf nitrogen (0.10) are similarly assumed constant across all plant growth strategies and are accounted for by parameter $c_{sapwood}$. The "seed" and storage carbon pools are not subject to maintenance respiration within the model, however, they do decay at a constant rate as described in Sect. A6.

A9   Scaling from plant growth strategies to community-aggregated fluxes

JeDi-DGVM calculates community-aggregated fluxes and land surface properties assuming the "biomass-ratio" hypothesis (Grime, 1998), i.e. as the mean over the individual plant growth strategies weighted by their mass-based relative abundances. The instantaneous relative abundance $p^*_{(i,j)}$ of a plant growth strategy i in a grid cell j is assumed to be proportional to its living biomass at that grid cell relative to the sum of the living biomass of all surviving growth strategies S in that grid cell. The living biomass $C_{tot(i,j)}$ of a growth strategy being the sum of its leaf, fine root, woody and storage carbon pools ($C_{tot(i,j)} = C_{A(i,j)} + C_{L(i,j)} + C_{R(i,j)} + C_{WL(i,j)} + C_{WR(i,j)}$).

$$
\begin{aligned}
p^*_{(i,j)} &= \frac{C_{tot(i,j)}}{\sum_{k=1}^{S} C_{tot(k,j)}} \\
\frac{dp_{(i,j)}}{dt} &= \frac{p^*_{(i,j)} - p_{(i,j)}}{\tau_p}
\end{aligned}
\tag{A21}
$$

The relative abundance $p_{(i,j)}$ used for the calculation of community-aggregated fluxes and properties relaxes towards the instantaneous relative abundance $p^*_{(i,j)}$ at time scale τ_p (= 365 days). This relaxation mechanism was necessary to alleviate numerical issues related to the conservation of mass. In the previous subsections describing the development of a individual plant growth strategies, we omitted this subscript notation to improve readability. Throughout the remainder of this appendix, we adopt chevron (angled bracket) notation to denote community-aggregated fluxes and properties. As an example, the community-aggregated gross primary productivity $\langle GPP_j \rangle$ for a given grid cell j is equal to the sum of the GPP fluxes of all the plant growth strategies S in that grid cell weighted by their respective mass-based relative abundances.

$$\langle GPP_j \rangle = \sum_{i=1}^{S} p_{(i,j)} GPP_{(i,j)} \tag{A22}$$

A10 Soil carbon

The soil carbon module in JeDi-DGVM is loosely based on the soil carbon component of the JSBACH land surface model (Raddatz et al., 2007; Thum et al., 2011). The parameters and variables of the soil carbon module are summarized in Table C5. The following differential equations describe the dynamics of the three detritus carbon pools, fine litter carbon C_{LIT}, woody litter carbon C_{CWD}, and soil carbon C_{SOIL}:

$$\frac{dC_{LIT}}{dt} = \langle LIT_L \rangle + \langle LIT_R \rangle + \langle LIT_A \rangle + \langle LIT_S \rangle - DEC_{LIT}$$

$$\frac{dC_{CWD}}{dt} = \langle LIT_{WL} \rangle + \langle LIT_{WR} \rangle - DEC_{CWD} \tag{A23}$$

$$\frac{dC_{SOIL}}{dt} = (1 - c_{lit \triangleright atm})DEC_{LIT} + (1 - c_{cwd \triangleright atm})DEC_{CWD} - DEC_{SOIL}$$

The soil carbon dynamics are not computed separately for each plant growth strategy. Instead, carbon enters the two common litter pools through the community-aggregated

Full Screen / Esc

Printer-friendly Version

Interactive Discussion

litter fluxes $\langle \mathrm{LIT_{tissue}} \rangle$ from the turnover of the various vegetation tissue pools.

$$\langle \mathrm{LIT_{tissue}} \rangle = \sum_{k=1}^{n} \left(p_{(k)} \frac{C_{\mathrm{tissue}(k)}}{\tau_{\mathrm{tissue}(k)}} \right) + \sum_{k=1}^{n} \left(C_{\mathrm{tissue}(k)} \max(0, -\Delta p_{(k)}) \right) \tag{A24}$$

$$\langle \mathrm{LIT_S} \rangle = \sum_{k=1}^{n} \frac{C_{\mathrm{S}(k)}}{\tau_{\mathrm{A}(k)}}$$

The second term in the calculation of $\langle \mathrm{LIT_{tissue}} \rangle$ is necessary to maintain the conservation of carbon when the relative abundance of a plant growth strategy decreases during the current time step. Likewise, the vegetation carbon pools (except the "seed" pool C_S) are scaled down when the relative abundance of a growth strategy increases during the current time step.

$$C_{\mathrm{tissue}(t)} = C_{\mathrm{tissue}(t-\Delta t)} \frac{p_{(t-\Delta t)}}{p_{(t-\Delta t)} + \max(0, \Delta p)} \tag{A25}$$

The decomposition fluxes DEC_x out of the detritus carbon pools are computed from the amount of carbon in that pool, a Q_{10} temperature response function, and a fixed turnover time for that pool at reference temperature 20 °C. The value of 1.4 for the sensitivity of heterotrophic respiration to air temperature $Q_{10,h}$ is taken from a recent global study of FLUXNET sites (Mahecha et al., 2010). Fixed fractions of the decomposition fluxes from the litter pools enter the common soil carbon pool.

$$\mathrm{DEC}_x = Q_{10,h}^{\left(\frac{T-20}{10} \right)} \frac{C_x}{\tau_x} \tag{A26}$$

The heterotrophic respiration flux $\mathrm{RES_h}$ to the atmosphere is estimated as the sum of the fractions of the decomposition fluxes from the litter pools not entering the soil carbon pool and the decomposition flux out of the soil carbon pool.

$$\mathrm{RES_h} = c_{\mathrm{lit \triangleright atm}} \mathrm{DEC_{LIT}} + c_{\mathrm{cwd \triangleright atm}} \mathrm{DEC_{CWD}} + \mathrm{DEC_{SOIL}} \tag{A27}$$

4674

Finally, the community-aggregated net ecosystem exchange NEE is calculated as the difference the heterotrophic respiration and the community-aggregated net primary productivity fluxes.

$$NEE = RES_h - \langle NPP \rangle \tag{A28}$$

Appendix B

Land-surface module

The land-surface hydrology module of JeDi-DGVM is largely based on the land-surface component of the ECHAM4 atmospheric General Circulation Model (Roeckner et al., 1996) along with modifications introduced by KM2000. It consists of four budget equations for water stored in the vegetation canopy W_L, in the snow cover W_S, in the rooting zone W, and below the rooting zone W_{SUB}:

$$\frac{dW_L}{dt} = P_{rain} - E_{can} - F_{thfall} \tag{B1}$$

$$\frac{dW_S}{dt} = P_{snow} - F_{melt} - E_{snow}$$

$$\frac{dW}{dt} = F_{thfall} + F_{melt} - F_{runoff} - E_{bare} - E_{trans} - F_{drain} - F_{\Delta Wmax}$$

$$\frac{dW_{SUB}}{dt} = F_{drain} - F_{subdrain} + F_{\Delta Wmax}$$

The variables and parameters of the land-surface module are summarized in Tables C6 and C7. The module runs on a daily time step using forcing variables: precipitation flux (P), near-surface air temperature (T), and downward shortwave and longwave radiation fluxes ($R_{sw\downarrow}$ and $R_{lw\downarrow}$). The various flux terms of the budget equations are described below. A schematic diagram of the land-surface module is shown in Fig. 18.

B1 Water storage and runoff generation

The partitioning of precipitation between snow P_{snow} and rain P_{rain} depends on near-surface air temperature T following Wigmosta et al. (1994).

$$P_{snow} = \begin{cases} P & T \leq -1.1 \\ P\frac{3.3-T}{4.4} & -1.1 < T < 3.3 \\ 0 & T \geq 3.3 \end{cases} \tag{B2}$$

$$P_{rain} = P - P_{snow}$$

Rainfall is first intercepted in the canopy reservoir W_L up to a maximum storage capacity W_{Lmax} which depends on LAI (see Eq. A11). If a precipitation event causes the water in the canopy reservoir to exceed its storage capacity, the excess water flows from the canopy reservoir to the rooting zone as throughfall F_{thfall}.

$$F_{thfall} = \max(0, W_L + P_{rain} - W_{Lmax}) \tag{B3}$$

Snowmelt F_{melt} is computed according to a day-degree formula using a melt rate of $3.22 \, \mathrm{mm \, days^{-1} \, {}^\circ C^{-1}}$ (Hagemann and Dümenil, 1997).

$$F_{melt} = \begin{cases} 0 & T < 0 \\ \min(3.22T, P_{snow} + W_S) & T \geq 0 \end{cases} \tag{B4}$$

Surface runoff F_{runoff} occurs when the throughfall or snowmelt fluxes cause the rooting zone reservoir to exceed its maximum capacity W_{MAX} (see Eq. A11).

$$F_{runoff} = \begin{cases} F_{thfall} & T \leq 0 \\ \max(0, W + F_{thfall} + F_{melt} - W_{max}) & T > 0 \end{cases} \tag{B5}$$

When the air temperature drops below $0\,{}^\circ C$, the soil is assumed to be frozen, inhibiting infiltration, and the entire throughfall flux becomes surface runoff.

Drainage from the rooting zone F_{drain} supplies water to the sub-rooting zone and depends on the soil wetness ($f_W = W/W_{MAX}$).

$$F_{drain} = \begin{cases} 0 & f_W \le 0.05 \\ d_{min} f_W & 0.05 < f_W < 0.9 \\ d_{min} f_W + (d_{max} - d_{min}) \left(\frac{f_W - 0.9}{1 - 0.9}\right)^d & f_W \ge 0.9 \end{cases} \tag{B6}$$

When the rooting zone is between 5 % and 90 % of field capacity, it drains slowly ($d_{min} = 0.24\,\text{mm days}^{-1}$) with a linear dependence on soil wetness. When the rooting zone nears saturation ($f_W \ge 0.9$), the drainage rate quickly increases with increasing wetness towards its maximum drainage rate ($d_{max} = 2.40\,\text{mm days}^{-1}$). Drainage from the rooting zone ceases when the soil wetness falls below 5 %.

When the incoming drainage from the overlying rooting zone F_{drain} causes the sub-rooting zone to exceed its maximum capacity ($W_{SUB,max}$), the excess flows out as sub-rooting zone drainage $F_{subdrain}$:

$$F_{subdrain} = \max(0, W_{SUB} + F_{drain} - (W_{SUB,max} - W_{max})) \tag{B7}$$

where $W_{SUB,max}$ is maximum storage capacity of the entire soil column.

The flux term $F_{\Delta W max}$ accounts for changes in the depth of the rooting zone W_{MAX} (see Eq. A11) due to the balance between carbon allocation to coarse root growth and the loss of coarse root biomass via turnover.

$$F_{\Delta W max} = \begin{cases} \Delta W_{max} \cdot \frac{W_{SUB}}{W_{SUB,max} - W_{max}} & \Delta W_{max} < 0 \\ \Delta W_{max} \cdot \frac{W}{W_{max}} & \Delta W_{max} > 0 \end{cases} \tag{B8}$$

Coarse root growth (i.e. an increase in the depth of the rooting zone W_{MAX}) leads to a virtual flow of water from the sub-rooting zone to the rooting zone. Likewise, a decrease in the depth of rooting zone due to coarse root turnover leads to a virtual flow of water from the rooting zone to the sub-rooting zone.

Jena Diversity DGVM

R. Pavlick et al.

B2 Potential evapotranspiration

The fractional snow area f_{SNOW} depends on the amount of water in the snow cover W_S:

$$f_{SNOW} = \min(1, \frac{W_S}{W_{Scrit}}) \tag{B9}$$

where $W_{S,crit}$ is the critical snow depth (water-equivalent). Following Robock (1980), the albedo of snow a_s depends on air temperature T and the fractional forest cover f_{FOR} (see Eq. A11).

$$a_{s,min} = 0.3f_{FOR} + 0.4(1 - f_{FOR})$$
$$a_{s,max} = 0.4f_{FOR} + 0.8(1 - f_{FOR})$$

$$a_s = \begin{cases} 0 & T \geq 0 \\ a_{s,max} - (a_{s,max} - a_{s,min})\frac{T+10}{10} & -10 < T < 0 \\ 1 & T \leq -10 \end{cases} \tag{B10}$$

The potential evapotranspiration fluxes for the snow-covered and snow-free fractions are estimated using the Priestley-Taylor equation (Priestley and Taylor, 1972) from the net radiation fluxes described below, the slope of the saturation-vapor pressure curve ϵ at air temperature T, the psychrometric constant Γ, the latent heat of vaporization λ, and the Priestley-Taylor coefficient α_p.

$$D_s = \alpha_p \frac{\epsilon(T)}{\epsilon(T) + \Gamma} \frac{R_{net,s}}{\lambda}$$
$$D_{ns} = \alpha_p \frac{\epsilon(T)}{\epsilon(T) + \Gamma} \frac{R_{net,ns}}{\lambda} \tag{B11}$$

The net radiative energy available for evaporative processes R_{net} is calculated separately for the snow-covered and snow-free fractions from the downward shortwave $R_{sw\downarrow}$

and net longwave R_{lw} radiation fluxes, daylength h, and the albedo of the respective fraction (a_s and a_{ns}).

$$R_{net,s} = f_{SNOW}86\,400\left(R_{sw\downarrow}(1 - a_s) + \frac{h}{86\,400}R_{lw}\right)$$

$$R_{net,ns} = (1 - f_{SNOW})86\,400\left(R_{sw\downarrow}(1 - a_{ns}) + \frac{h}{86\,400}R_{lw}\right) \quad \text{(B12)}$$

Net longwave radiation R_{lw} is the sum of the downward longwave radiation forcing $R_{lw\downarrow}$ and upward longwave radiation $R_{lw\uparrow}$ estimated from the near-surface air temperature in Kelvin ($T_K = T + 273.16$) using the Stefan-Boltzmann equation:

$$R_{lw\uparrow} = \epsilon\sigma T_K{}^4 \quad \text{(B13)}$$

where ϵ is the average emissivity of land surfaces (Brutsaert, 1982) and σ is the Stefan-Boltzmann constant.

B3 Actual evapotranspiration

B3.1 Sublimation from snow cover

Sublimation from snow E_{snow} is taken as the minimum of the potential evaporation rate for the snow-covered fraction D_s and the supply of water in the snow cover W_S.

$$F_{sublim} = \min(D_s, W_S) \quad \text{(B14)}$$

B3.2 Evaporation from canopy interception reservoir

Similarly, evaporation from the canopy reservoir E_{can} is taken as the minimum of the potential evapotranspiration rate for the snow-free fraction and the supply of water in the canopy W_L.

$$E_{can} = \min(D_{ns}, W_L) \quad \text{(B15)}$$

B3.3 Bare soil evaporation

Bare soil evaporation E_{bare} occurs in the fraction of the snow-free area not covered by vegetation $(1 - f_{VEG})$ and declines linearly within decreasing soil moisture.

$$E_{bare} = \min \begin{cases} b(1 - f_{VEG})(D_{ns} - E_{can}) \\ W \end{cases} \tag{B16}$$

$$b = \begin{cases} 0.5 \left[1 - \cos \left(\pi \frac{W - (W_{max} - W_{top})}{W_{top}} \right) \right] & W \geq W_{max} - W_{top} \\ 0 & W < W_{max} - W_{top} \end{cases}$$

$$\tag{B17}$$

The factor b limits soil evaporation to the water in the top 50 mm of the rooting zone (W_{top}).

B3.4 Transpiration

Transpiration E_{trans} is reduced by factor α_{H_2O} from Eq. (A18), which is a saturating function of the available supply for transpiration S and the the atmospheric demand for transpiration $(D_{ns} - E_{can})$.

$$E_{trans} = \min \begin{cases} \alpha_{H_2O} f_{VEG}(D_{ns} - E_{can}) \\ W - E_{bare} \end{cases} \tag{B18}$$

B4 Approximation of latent and sensible heat fluxes

The total evapotranspiration flux ET is calculated as the sum of evaporation from the canopy reservoir and bare soil, sublimation from snow, and transpiration by

the vegetation.

$$\mathrm{ET} = E_{\mathrm{can}} + E_{\mathrm{bare}} + E_{\mathrm{snow}} + E_{\mathrm{trans}}$$
$$L = \lambda \mathrm{ET}$$
$$R_{\mathrm{net}} = f_{\mathrm{SNOW}} R_{\mathrm{net,s}} + (1 - f_{\mathrm{SNOW}}) R_{\mathrm{net,ns}} \tag{B19}$$
$$H = R_{\mathrm{net}} - L$$

The latent heat flux L is estimated by multiplying the evapotranspiration flux by the latent heat of vaporization for water λ. Total net radiation R_{net} is computed as the weighted combination of the net radiation over snow-covered and snow-free areas. Sensible heat H is assumed to make up the difference between the net radiation and latent heat fluxes.

Appendix C

Model parameters and variables

References

Ackerly, D. and Cornwell, W. K.: A trait-based approach to community assembly: partitioning of species trait values into within- and among-community components, Ecol. Lett., 10, 135–145, 2007. 4630, 4658

5   Ainsworth, E. A. and Long, S. P.: What have we learned from 15 years of free-air CO_2 enrichment (FACE)? A meta-analytic review of the responses of photosynthesis, canopy properties and plant production to rising CO_2, New Phytol., 165, 351–372, 2004. 4657

Alton, P. B.: How useful are plant functional types in global simulations of the carbon, water, and energy cycles?, J. Geophys. Res., 116, 1–13, 2011. 4630

10   Alvarado, V. and Bradford, K.: A hydrothermal time model explains the cardinal temperatures for seed germination, Plant Cell Environ., 25, 1061–1069, 2002. 4665

Arora, V. and Boer, G.: Simulating competition and coexistence between plant functional types in a dynamic vegetation model, Earth Interact., 10, 1–30, 2006. 4637

Asner, G. P. and Alencar, A.: Drought impacts on the Amazon forest: the remote sensing per-

15   spective, New Phytol., 187, 569–578, 2010. 4646

Axelsson, E. and Axelsson, B.: Changes in carbon allocation patterns in spruce and pine trees following irrigation and fertilization, Tree Physiol., 2, 189–204, 1986. 4657

Baas-Becking, L.: Geobiologie of Inleiding tot de Milieukunde, van Stockum and Zoon, The Hague, Netherlands, 1934. 4632

20   Baker, D., Law, R., Gurney, K., Rayner, P., Peylin, P., Denning, A., Bousquet, P., Bruhwiler, L., Chen, Y., Ciais, P., Fung, I., Heimann, M., John, J., Maki, T., Maksyutov, S., Masarie, K., Prather, M., Pak, B., Taguchi, S., and Zhu, Z.: TransCom 3 inversion intercomparison: impact of transport model errors on the interannual variability of regional CO_2 fluxes, 1988–2003, Global Biogeochem. Cy., 20, GB1002, doi:10.1029/2004GB002439, 2006. 4641, 4642, 4722

25   Beer, C., Reichstein, M., Tomelleri, E., Ciais, P., Jung, M., Carvalhais, N., Rodenbeck, C., Arain, M. A., Baldocchi, D. D., Bonan, G., Bondeau, A., Cescatti, A., Lasslop, G., Lindroth, A., Lomas, M., Luyssaert, S., Margolis, H., Oleson, K. W., Roupsard, O., Veenendaal, E., Viovy, N., Williams, C., Woodward, F. I., and Papale, D.: Terrestrial gross carbon dioxide uptake: global distribution and covariation with climate, Science, 329, 834–838, 2010.

30   4641, 4647, 4715, 4716

Bloom, A. J., Chapin, F. S. I., and Mooney, H.: Resource limitation in plants – an economic analogy, Annu. Rev. Ecol. Syst., 16, 363–392, 1985. 4632

Title Page

Abstract	Introduction
Conclusions	References
Tables	Figures

◄ | ►

◄ | ►

Back | Close

Full Screen / Esc

Printer-friendly Version

Interactive Discussion

Bohn, K., Dyke, J. G., Pavlick, R., Reineking, B., Reu, B., and Kleidon, A.: The relative importance of seed competition, resource competition and perturbations on community structure, Biogeosciences, 8, 1107–1120, doi:10.5194/bg-8-1107-2011, 2011. 4657, 4658

Bonan, G. and Levis, S.: Evaluating aspects of the community land and atmosphere models (CLM3 and CAM3) using a dynamic global vegetation model, J. Climate, 19, 2290–2301, 2006. 4649

Bonan, G., Levis, S., Kergoat, L., and Oleson, K. W.: Landscapes as patches of plant functional types: an integrating concept for climate and ecosystem models, Global Biogeochem. Cy., 16, 1–18, 2002. 4630

Box, E.: Plant functional types and climate at the global scale, J. Veg. Sci., 7, 309–320, 1996. 4630

Bruggeman, J. and Kooijman, S.: A biodiversity-inspired approach to aquatic ecosystem modeling, Limnol. Oceanogr., 52, 1533–1544, 2007. 4631

Brutsaert, W.: Evaporation into the Atmosphere, Theory, History, and Applications, Kluwer Academic Publishers, Dordrecht, The Netherlands, 1982. 4679

Cannell, M. G. R.: World Forest Biomass and Primary Production Data, Academic Press, London, UK, 1982. 4658

Cannell, M. G. R. and Thornley, J.: Temperature and CO_2 responses of leaf and canopy photosynthesis: a clarification using the non-rectangular hyperbola model of photosynthesis, Ann. Bot.-London, 82, 883–892, 1998. 4671

Cavender-Bares, J., Kozak, K. H., Fine, P. V. A., and Kembel, S. W.: The merging of community ecology and phylogenetic biology, Ecol. Lett., 12, 693–715, 2009. 4656

Chapin, F. S. I., BretHarte, M., Hobbie, S., and Zhong, H.: Plant functional types as predictors of transient responses of arctic vegetation to global change, J. Veg. Sci., 7, 347–358, 1996. 4630

Chave, J., Coomes, D., Jansen, S., Lewis, S. L., Swenson, N. G., and Zanne, A. E.: Towards a worldwide wood economics spectrum, Ecol. Lett., 12, 351–366, 2009. 4658

Cohen, D.: A general model of optimal reproduction in a randomly varying Eevironment, J. Ecol., 56, 219–228, 1968. 4665

Cornwell, W. K. and Ackerly, D.: Community assembly and shifts in plant trait distributions across an environmental gradient in coastal California, Ecol. Monogr., 79, 109–126, 2009. 4658

Title Page

Abstract | Introduction

Conclusions | References

Tables | Figures

◄ | ►

◄ | ►

Back | Close

Full Screen / Esc

Printer-friendly Version

Interactive Discussion

Cox, P.: Description of the TRIFFID Dynamic Global Vegetation Model, Hadley Centre, Bracknell, UK, 2001. 4629, 4637

Cox, P., Betts, R. A., Jones, C. D., Spall, S. A., and Totterdell, I. J.: Acceleration of global warming due to carbon-cycle feedbacks in a coupled climate model, Nature, 408, 184–187, 2000. 4629, 4630

Cramer, W., Bondeau, A., Woodward, F. I., Prentice, I. C., Betts, R. A., Brovkin, V., Cox, P., Fisher, V., Foley, J. A., Friend, A. D., Kucharik, C., Lomas, M. R., Ramankutty, N., Sitch, S., Smith, B., White, A., and Young-Molling, C.: Global response of terrestrial ecosystem structure and function to CO_2 and climate change: results from six dynamic global vegetation models, Glob. Change Biol., 7, 357–373, 2001. 4647

Denman, K., Brasseur, G., Chidthaisong, A., Ciais, P., Cox, P., Dickinson, R., Hauglustaine, D., Heinze, C., Holland, E., Jacob, D., Lohmann, U., Ramachandran, S., da Silva Dias, P., Wofsy, S. C., and Zhang, X.: Couplings between changes in the climate system and biogeochemistry, Climate Change 2007: The Physical Science Basis, Contribution of Working Group I to the Fourth Assessment Report of the Intergovernmental Panel on Climate Change, Cambridge, United Kingdom, 2007. 4650

Díaz, S. and Cabido, M.: Vive la différence: plant functional diversity matters to ecosystem processes, Trends Ecol. Evol., 16, 646–655, 2001. 4630

Díaz, S., Fargione, J., Chapin, F. S., and Tilman, D.: Biodiversity loss threatens human well-being, PLoS Biol., 4, 1300–1305, 2006. 4630

Díaz, S., Lavorel, S., de Bello, F., Quetier, F., Grigulis, K., and Robson, T. M.: Incorporating plant functional diversity effects in ecosystem service assessments, in: Proceedings of the National Academy of Sciences, 104, 20684–20689, 2007. 4637, 4656

Doney, S., Lindsay, K., Fung, I., and John, J.: Natural variability in a stable, 1000-yr global coupled climate–carbon cycle simulation, J. Climate, 19, 3033–3054, 2006. 4639

Drewry, D., Kumar, P., Long, S., Bernacchi, C., Liang, X., and Sivapalan, M.: Ecohydrological responses of dense canopies to environmental variability: 1. interplay between vertical structure and photosynthetic pathway, J. Geophys. Res., 115, G04022, doi:10.1029/2010JG001340, 2010. 4651

Dunne, K. and Willmott, C.: Global distribution of plant extractable water capacity of soil, Int. J. Climatol., 16, 841–859, 1996. 4670

Dutkiewicz, S., Follows, M. J., and Bragg, J. G.: Modeling the coupling of ocean ecology and biogeochemistry, Global Biogeochem. Cy., 23, GB4017, doi:10.1029/2008GB003405, 2009. 4631

Elser, J. J., Bracken, M. E. S., Cleland, E. E., Gruner, D. S., Harpole, W. S., Hillebrand, H., Ngai, J. T., Seabloom, E. W., Shurin, J. B., and Smith, J. E.: Global analysis of nitrogen and phosphorus limitation of primary producers in freshwater, marine and terrestrial ecosystems, Ecol. Lett., 10, 1135–1142, 2007. 4648

Ezoe, H.: Optimal dispersal range and seed size in a stable environment, J. Theor. Biol., 190, 287–293, 1998. 4656

Falge, E., Baldocchi, D. D., Tenhunen, J., Aubinet, M., Bakwin, P., Berbigier, P., Bernhofer, C., Burba, G., Clement, R., Davis, K. J., Elbers, J. A., Goldstein, A. H., Grelle, A., Granier, A., Guomundsson, J., Hollinger, D., Kowalski, A. S., Katul, G., Law, B. E., Malhi, Y., Meyers, T., Monson, R. K., Munger, J. W., Oechel, W., Paw U, K. T., Pilegaard, K., Rannik, Ü., Rebmann, C., Suyker, A., Valentini, R., Wilson, K., and Wofsy, S.: Seasonality of ecosystem respiration and gross primary production as derived from FLUXNET measurements, Agr. Forest Meteorol., 113, 53–74, 2002. 4643

Falster, D. S., Brännström, Å., Dieckmann, U., and Westoby, M.: Influence of four major plant traits on average height, leaf-area cover, net primary productivity, and biomass density in single-species forests: a theoretical investigation, J. Ecol., 99, 148–164, 2010. 4631, 4658

Figueira, A. M. E. S., Miller, S. D., de Sousa, C. A. D., Menton, M. C., Maia, A. R., da Rocha, H. R., and Goulden, M. L.: Effects of selective logging on tropical forest tree growth, J. Geophys. Res.-Biogeo., 113, G00B05, doi:10.1029/2007JG000577, 2008. 4652

Fisher, J., Sitch, S., Malhi, Y., and Fisher, R.: Carbon cost of plant nitrogen acquisition: a mechanistic, globally applicable model of plant nitrogen uptake, retranslocation, and fixation, Global Biogeochem. Cy.,187, 666–681, 2010. 4648

Fisher, R., Williams, M., Lola da Costa, A., Malhi, Y., Lola da Costa, R. F., Almeida, S., and Meir, P.: The response of an Eastern Amazonian rain forest to drought stress: results and modelling analyses from a throughfall exclusion experiment, Glob. Change Biol., 13, 2361–2378, 2007. 4657

Fisher, R., McDowell, N., Purves, D., Moorcroft, P., Sitch, S., Cox, P., Huntingford, C., Meir, P., and Woodward, F. I.: Assessing uncertainties in a second-generation dynamic vegetation model caused by ecological scale limitations, New Phytol., 187, 666–681, 2010. 4629, 4631, 4657

Foley, J. A., Prentice, I. C., Ramankutty, N., Levis, S., Pollard, D., Sitch, S., and Haxeltine, A.: An integrated biosphere model of land surface processes, terrestrial carbon balance, and vegetation dynamics, Global Biogeochem. Cy., 10, 603–628, 1996. 4629

Foley, J. A., Levis, S., Costa, M., Cramer, W., and Pollard, D.: Incorporating dynamic vegetation cover within global climate models, Ecol. Appl., 10, 1620–1632, 2000. 4629

Follows, M. J. and Dutkiewicz, S.: Modeling diverse communities of marine microbes, Ann. Rev. Mar. Sci., 3(3), 427–451, 2011. 4631

Follows, M. J., Dutkiewicz, S., Grant, S., and Chisholm, S. W.: Emergent biogeography of microbial communities in a model ocean, Science, 315, 1843–1846, 2007. 4631

France, K. E. and Duffy, J. E.: Diversity and dispersal interactively affect predictability of ecosystem function, Nature, 441, 1139–1143, 2006. 4659

Franklin, O.: Optimal nitrogen allocation controls tree responses to elevated CO_2, New Phytol., 174, 811–822, 2007. 4670

Freschet, G. T., Dias, A. T. C., Ackerly, D., Aerts, R., Van Bodegom, P. M., Cornwell, W. K., Dong, M., Kurokawa, H., Liu, G., Onipchenko, V. G., Ordoñez, J. C., Peltzer, D. A., Richardson, S. J., Shidakov, I. I., Soudzilovskaia, N. A., Tao, J., and Cornelissen, J. H. C.: Global to community scale differences in the prevalence of convergent over divergent leaf trait distributions in plant assemblages, Global Ecol. Biogeogr., 20, 755–765, 2011. 4656

Friedlingstein, P., Joel, G., Field, C. B., and Fung, I. Y.: Toward an allocation scheme for global terrestrial carbon models, Glob. Change Biol., 5, 755–770, 1999. 4631

Friedlingstein, P., Cox, P., Betts, R. A., Bopp, L., von Bloh, W., Brovkin, V., Cadule, P., Doney, S., Eby, M., Fung, I., Bala, G., John, J., Jones, C., Joos, F., Kato, T., Kawamiya, M., Knorr, W., Lindsay, K., Matthews, H. D., Raddatz, T., Rayner, P., Reick, C., Roeckner, E., Schnitzler, K. G., Schnur, R., Strassmann, K., Weaver, A. J., Yoshikawa, C., and Zeng, N.: Climate-carbon cycle feedback analysis: results from the C 4MIP model intercomparison, J. Climate, 19, 3337–3353, 2006. 4629, 4639

Friend, A., Stevens, A., Knox, R., and Cannell, M.: A process-based, terrestrial biosphere model of ecosystem dynamics (Hybrid v3.0), Ecol. Model., 95, 249–287, 1997. 4629

Fung, I. Y., Doney, S., Lindsay, K., and John, J.: Evolution of carbon sinks in a changing climate, in: Proceedings of the National Academy of Sciences of the United States of America, 102, 11201–11206, 2005. 4639

Garnier, E., Cortez, J., Billes, G., Navas, M., Roumet, C., Debussche, M., Laurent, G., Blanchard, A., Aubry, D., Bellmann, A., Neill, C., and Toussaint, J.: Plant functional markers cap-

ture ecosystem properties during secondary succession, Ecology, 85, 2630–2637, 2004. 4637, 4656

Grime, J.: Benefits of plant diversity to ecosystems: immediate, filter and founder effects, J. Ecol., 86, 902–910, 1998. 4633, 4637, 4672

5   Groenendijk, M., Dolman, A. J., van der Molen, M. K., Leuning, R., Arneth, A., Delpierre, N., Gash, J. H. C., Lindroth, A., Richardson, A. D., and Verbeeck, H.: Assessing parameter variability in a photosynthesis model within and between plant functional types using global fluxnet eddy covariance data, Agr. Forest Meteorol., 151, 22–38, 2011. 4630

Gu, L., Baldocchi, D. D., Wofsy, S. C., Munger, J. W., Michalsky, J., Urbanski, S., and Boden, T.:
10   Response of a deciduous forest to the Mount Pinatubo eruption: enhanced photosynthesis, Science, 299, 2035–2038, 2003. 4651

Gurney, K., Law, R., Denning, A., Rayner, P., Pak, B., Baker, D., Bousquet, P., Bruhwiler, L., Chen, Y., Ciais, P., Fung, I., Heimann, M., John, J., Maki, T., Maksyutov, S., Peylin, P., Prather, M., and Taguchi, S.: Transcom 3 inversion intercomparison: model mean results for
15   the estimation of seasonal carbon sources and sinks, Global Biogeochem. Cy., 18, GB1010, doi:10.1029/2003GB002111, 2004. 4641, 4720, 4721

Haddeland, I., Clark, D. B., Franssen, W., Ludwig, F., Voß, F., Arnell, N. W., Bertrand, N., Best, M., Folwell, S., Gerten, D., Gomes, S., Gosling, S. N., Hagemann, S., Hanasaki, N., Harding, R., Heinke, J., Kabat, P., Koirala, S., Oki, T., Polcher, J., Stacke, T., Viterbo, P., Wee-
20   don, G. P., and Yeh, P.: Multimodel estimate of the global terrestrial water balance: setup and first results, J. Hydrometeorol., 12, 869–884, 2011. 4648

Hagemann, S. and Dümenil, L.: A parametrization of the lateral waterflow for the global scale, Clim. Dynam., 14, 17–31, 1997. 4676

Hall, C., Stanford, J., and Hauer, F.: The distribution and abundance of organisms as a con-
25   sequence of energy balances along multiple environmental gradients, Oikos, 65, 377–390, 1992. 4632

Harrison, S. P., Prentice, I. C., Barboni, D., Kohfeld, K. E., Ni, J., and Sutra, J.-P.: Ecophysio-logical and bioclimatic foundations for a global plant functional classification, J. Veg. Sci., 21, 300–317, 2010. 4629, 4630, 4631

30   Hartmann, D. L.: Global Physical Climatology, International Geophysics Series, 1st edn., Aca-demic Press, San Francisco, 1994. 4671

Heinsch, F., Zhao, M., Running, S. W., Kimball, J. S., Nemani, R. R., Davis, K. J., Bolstad, P. V., Cook, B. D., Desai, A. R., Ricciuto, D. M., Law, B. E., Oechel, W. C., Kwon, H., Luo, H.,

Wofsy, S. C., Dunn, A. L., Munger, J. W., Baldocchi, D. D., Xu, L., Hollinger, D. Y., Richardson, A. D., Stoy, P. C., Siqueira, M. B. S., Monson, R. K., Burns, S. P., and Flanagan, L. B.: Evaluation of remote sensing based terrestrial productivity from MODIS using regional tower eddy flux network observations, IEEE T. Geosci. Remote, 44, 1908–1925, 2006. 4640, 4643, 4715, 4718

Hickler, T., Prentice, I. C., Smith, B., Sykes, M. T., and Zaehle, S.: Implementing plant hydraulic architecture within the LPJ dynamic global vegetation model, Global Ecol. Biogeogr., 15, 567–577, 2006. 4658

Hickler, T., Smith, B., Prentice, I. C., Mjöfors, K., Miller, P., Arneth, A., and Sykes, M. T.: CO_2 fertilization in temperate FACE experiments not representative of boreal and tropical forests, Glob. Change Biol., 14, 1531–1542, 2008. 4653

Hollinger, D. Y., Ollinger, S. V., Richardson, A. D., Meyers, T. P., Dail, D. B., Martin, M. E., Scott, N. A., Arkebauer, T. J., Baldocchi, D. D., Clark, K. L., Curtis, P. S., Davis, K. J., Desai, A. R., Dragoni, D., Goulden, M. L., Gu, L., Katul, G. G., Pallardy, S. G., Paw U, K. T., Schmid, H. P., Stoy, P. C., Sukyer, A. E., and Verma, S. B.: Albedo estimates for land surface models and support for a new paradigm based on foliage nitrogen concentration, Glob. Change Biol., 16, 696–710, 2010. 4669

Houghton, R. A., Hall, F., and Goetz, S. J.: Importance of biomass in the global carbon cycle, J. Geophys. Res., 114, G00E03, doi:10.1029/2009JG000935, 2009. 4647

Hubbell, S. P.: Tree dispersion, abundance, and diversity in a tropical dry forest, Science, 203, 1299–1309, 1979. 4645

Hubbell, S. P.: A unified theory of biogeography and relative species abundance and its application to tropical rain forests and coral reefs, Coral Reefs, 16, 9–21, 1997. 4645

Ito, A.: A historical meta-analysis of global terrestrial net primary productivity: are estimates converging?, Glob. Change Biol., 17, 3161–3175, 2011. 4647

Ives, A. R. and Carpenter, S. R.: Stability and diversity of ecosystems, Science, 317, 58–62, 2007. 4659

Jackson, S. and Williams, J.: Modern analogs in quaternary paleoecology: here today, gone yesterday, gone tomorrow?, Annu. Rev. Earth Pl. Sc., 32, 495–537, 2004. 4631, 4659

Johnson, I. R. and Thornley, J. H. M.: A model of instantaneous and daily canopy photosynthesis, J. Theor. Biol., 107, 531–545, 1984. 4670

Title Page

Abstract | Introduction

Conclusions | References

Tables | Figures

◀ | ▶

◀ | ▶

Back | Close

Full Screen / Esc

Printer-friendly Version

Interactive Discussion

Jung, M., Reichstein, M., and Bondeau, A.: Towards global empirical upscaling of FLUXNET eddy covariance observations: validation of a model tree ensemble approach using a biosphere model, Biogeosciences, 6, 2001–2013, doi:10.5194/bg-6-2001-2009, 2009. 4641

Jung, M., Reichstein, M., Ciais, P., Seneviratne, S. I., Sheffield, J., Goulden, M. L., Bonan, G., Cescatti, A., Chen, J., de Jeu, R., Dolman, A. J., Eugster, W., Gerten, D., Gianelle, D., Gobron, N., Heinke, J., Kimball, J., Law, B. E., Montagnani, L., Mu, Q., Mueller, B., Oleson, K. W., Papale, D., Richardson, A. D., Roupsard, O., Running, S., Tomelleri, E., Viovy, N., Weber, U., Williams, C., Wood, E. F., Zaehle, S., and Zhang, K.: Recent decline in the global land evapotranspiration trend due to limited moisture supply, Nature, 467, 951–954, 2010. 4641, 4648, 4649, 4715, 4719

Kaduk, J. and Heimann, M.: Assessing the climate sensitivity of the global terrestrial carbon cycle model SILVAN, Phys. Chem. Earth, 21, 529–535, 1996. 4661

Kattge, J., Knorr, W., Raddatz, T. J., and Wirth, C.: Quantifying photosynthetic capacity and its relationship to leaf nitrogen content for global-scale terrestrial biosphere models, Glob. Change Biol., 15, 976–991, 2009. 4631

Kattge, J., Díaz, S., Lavorel, S., Prentice, I. C., Leadley, P., Bönisch, G., Garnier, E., Westoby, M., Reich, P., Wright, I. J., Cornelissen, J. H. C., Violle, C., Harrison, S., van Bodegom, P., Reichstein, M., Enquist, B., Soudzilovskaia, N., Ackerly, D., Anand, M., Atkin, O., Bahn, M., Baker, T., Baldocchi, D. D., Bekker, R., Blanco, C., Blonder, B., Bond, W., Bradstock, R., Bunker, D., Casanoves, F., Cavender-Bares, J., Chambers, J. Q., Chapin, F. S. I., Chave, J., Coomes, D., Cornwell, W., Craine, J., Dobrin, B., Duarte, L., Durka, W., Elser, J., Esser, G., Estiarte, M., Fagan, W., Fang, J., Fernández-Méndez, F., Fidelis, A., Finegan, B., Flores, O., Ford, H., Frank, D., Freschet, G., Fyllas, N., Gallagher, R., Green, W., Gutierrez, A., Hickler, T., Higgins, S. L., Hodgson, J., Jalili, A., Jansen, S., Joly, C., Kerkhoff, A., Kirkup, D., Kitajima, K., Kleyer, M., Klotz, S., Knops, J., Kramer, K., Kühn, I., Kurokawa, H., Laughlin, D., Lee, T., Leishman, M., Lens, F., Lenz, T., Lewis, S., Lloyd, J., Llusià, J., Louault, F., Ma, S., Mahecha, M., Manning, P., Massad, T., Medlyn, B., Messier, J., Moles, A., Müller, S., Nadrowski, K., Naeem, S., Niinemets, Ü., Nöllert, S., Nüske, A., Ogaya, R., Oleksyn, J., Onipchenko, V., Onoda, Y., Ordoñez, J., Overbeck, G., Ozinga, W., Patiño, S., Paula, S., Pausas, J., Peñuelas, J., Phillips, O., Pillar, V., Poorter, H., Poorter, L., Poschlod, P., Prinzing, A., Proulx, R., Rammig, A., Reinsch, S., Reu, B., Sack, L., Salgado-Negret, B., Sardans, J., Shiodera, S., Shipley, B., Siefert, A., Sosinski, E., Soussana, J.-F., Swaine, E., Swenson, N., Thompson, K., Thornton, P., Waldram, M., Weiher, E., White, M., White, S.,

Title Page

Abstract | Introduction

Conclusions | References

Tables | Figures

◀ | ▶

◀ | ▶

Back | Close

Full Screen / Esc

Printer-friendly Version

Interactive Discussion

Wright, J., Yguel, B., Zaehle, S., Zanne, A., and Wirth, C.: TRY – a global database of plant traits, Glob. Change Biol., 17, 2905–2935, 2011. 4629, 4630, 4655, 4657, 4667

Kazakou, E., Vile, D., Shipley, B., Gallet, C., and Garnier, E.: Co-variations in litter decomposition, leaf traits and plant growth in species from a mediterranean old-field succession, Funct. Ecol., 20, 21–30, 2006. 4637, 4656

Kleidon, A. and Mooney, H.: A global distribution of biodiversity inferred from climatic constraints: results from a process-based modelling study, Glob. Change Biol., 6, 507–523, 2000. 4632

Kleidon, A., Fraedrich, K., and Low, C.: Multiple steady-states in the terrestrial atmosphere-biosphere system: a result of a discrete vegetation classification?, Biogeosciences, 4, 707–714, doi:10.5194/bg-4-707-2007, 2007. 4630

Kleidon, A., Adams, J., Pavlick, R., and Reu, B.: Simulated geographic variations of plant species richness, evenness and abundance using climatic constraints on plant functional diversity, Environ. Res. Lett., 4, 1, doi:10.1088/1748-9326/4/1/014007, 2009. 4632

Kleinen, T., Brovkin, V., and Schuldt, R. J.: A dynamic model of wetland extent and peat accumulation: results for the Holocene, Biogeosciences, 9, 235–248, doi:10.5194/bg-9-235-2012, 2012. 4650

Knorr, W. and Heimann, M.: Impact of drought stress and other factors on seasonal land biosphere CO_2 exchange studied through an atmospheric tracer transport model, Tellus B, 47, 471–489, 1995. 4661

Kraft, N. J. B., Valencia, R., and Ackerly, D.: Functional traits and niche-based tree community assembly in an Amazonian forest, Science, 322, 580–582, 2008. 4656

Kraft, N. J. B., Comita, L. S., Chase, J. M., Sanders, N. J., Swenson, N. G., Crist, T. O., Stegen, J. C., Vellend, M., Boyle, B., Anderson, M. J., Cornell, H. V., Davies, K. F., Freestone, A. L., Inouye, B. D., Harrison, S. P., and Myers, J. A.: Disentangling the drivers of diversity along latitudinal and elevational gradients, Science, 333, 1755–1758, 2011. 4656

Kreft, H. and Jetz, W.: Global patterns and determinants of vascular plant diversity, in: Proceedings of the National Academy of Sciences, 104, 5925–5930, 2007. 4644

Krinner, G., Viovy, N., de Noblet-Ducoudré, N., Ogée, J., Polcher, J., Friedlingstein, P., Ciais, P., Sitch, S., and Prentice, I. C.: A dynamic global vegetation model for studies of the coupled atmosphere-biosphere system, Global Biogeochem. Cy., 19, 1–33, 2005. 4647

Laughlin, D., Fulé, P., Huffman, D., Crouse, J., and Laliberté, E.: Climatic constraints on trait-based forest assembly, J. Ecol., 99, 1489–1499, 2011. 4638

LeBauer, D. S. and Treseder, K. K.: Nitrogen limitation of net primary productivity in terrestrial ecosystems is globally distributed, Ecology, 89, 371–379, 2008. 4648

Lee, E.: Impacts of meteorology-driven seed dispersal on plant migration: implications for future vegetation structure under changing climates, PhD thesis, Massachusetts Institute of Technology, Cambridge, Massachusetts, 2011. 4655

Lee, J.-E., Oliveira, R. S., Dawson, T. E., and Fung, I.: Root functioning modifies seasonal climate, in: Proceedings of the National Academy of Sciences of the United States of America, 102, 17576–17581, 2005. 4656

Liang, M. and Xie, Z.: Improving the vegetation dynamic simulation in a land surface model by using a statistical-dynamic canopy interception scheme, Adv. Atmos. Sci., 25, 610–618, 2008. 4649

Litchman, E., Klausmeier, C. A., Schofield, O. M., and Falkowski, P. G.: The role of functional traits and trade-offs in structuring phytoplankton communities: scaling from cellular to ecosystem level, Ecol. Lett., 10, 1170–1181, 2007. 4631

Litton, C. M. and Giardina, C.: Below-ground carbon flux and partitioning: global patterns and response to temperature, Funct. Ecol., 22, 941–954, 2008. 4658

Litton, C. M., Raich, J. W., and Ryan, M. G.: Carbon allocation in forest ecosystems, Glob. Change Biol., 13, 2089–2109, 2007. 4658

Loehle, C.: Height growth rate trade-offs determine northern and southern range limits for trees, J. Biogeogr., 25, 735–742, 1998. 4631

Loreau, M.: Biodiversity and ecosystem functioning: current knowledge and future challenges, Science, 294, 804–808, 2001. 4659

Luyssaert, S., Inglima, I., Jung, M., Richardson, A. D., Reichsteins, M., Papale, D., Piao, S. L., Schulzes, E. D., Wingate, L., Matteucci, G., Aragao, L., Aubinet, M., Beers, C., Bernhoffer, C., Black, K. G., Bonal, D., Bonnefond, J. M., Chambers, J., Ciais, P., Cook, B., Davis, K. J., Dolman, A. J., Gielen, B., Goulden, M., Grace, J., Granier, A., Grelle, A., Griffis, T., Gruenwald, T., Guidolotti, G., Hanson, P. J., Harding, R., Hollinger, D. Y., Hutyra, L. R., Kolar, P., Kruijt, B., Kutsch, W., Lagergren, F., Laurila, T., Law, B. E., Le Maire, G., Lindroth, A., Loustau, D., Malhi, Y., Mateus, J., Migliavacca, M., Misson, L., Montagnani, L., Moncrieff, J., Moors, E., Munger, J. W., Nikinmaa, E., Ollinger, S. V., Pita, G., Rebmann, C., Roupsard, O., Saigusa, N., Sanz, M. J., Seufert, G., Sierra, C., Smith, M. L., Tang, J., Valentini, R., Vesala, T., and Janssens, I. A.: CO_2 balance of boreal, temperate, and tropical forests derived from a global database, Glob. Change Biol., 13, 2509–2537, 2007. 4658

Title Page

Abstract Introduction

Conclusions References

Tables Figures

◄ ►

◄ ►

Back Close

Full Screen / Esc

Printer-friendly Version

Interactive Discussion

Mahecha, M. D., Reichstein, M., Carvalhais, N., Lasslop, G., Lange, H., Seneviratne, S. I., Vargas, R., Ammann, C., Arain, M. A., Cescatti, A., Janssens, I. A., Migliavacca, M., Montagnani, L., and Richardson, A. D.: Global convergence in the temperature sensitivity of respiration at ecosystem level, Science, 329, 838–840, 2010. 4674

Malcolm, J., Markham, A., Neilson, R., and Garaci, M.: Estimated migration rates under scenarios of global climate change, J. Biogeogr., 29, 835–849, 2002. 4655

Malhi, Y., Aragao, L. E. O. C., Metcalfe, D. B., Paiva, R., Quesada, C. A., Almeida, S., Anderson, L., Brando, P., Chambers, J. Q., da Costa, A. C. L., Hutyra, L. R., Oliveira, P., Patiño, S., Pyle, E. H., Robertson, A. L., and Teixeira, L. M.: Comprehensive assessment of carbon productivity, allocation and storage in three Amazonian forests, Glob. Change Biol., 15, 1255–1274, 2009. 4643, 4652, 4657, 4724

Malhi, Y., Doughty, C., and Galbraith, D.: The allocation of ecosystem net primary productivity in tropical forests, Philos. T. R. Soc. B, 366, 3225–3245, 2011. 4658

Marks, C. O.: The causes of variation in tree seedling traits: the roles of environmental selection versus chance, Evolution, 61, 455–469, 2007. 4645

Marks, C. O. and Lechowicz, M. J.: A holistic tree seedling model for the investigation of functional trait diversity, Ecol. Model., 193, 141–181, 2006. 4645

Masarie, K. A. and Tans, P. P.: Extension and integration of atmospheric carbon dioxide data into a globally consistent measurement record, J. Geophys. Res., 100, 11593–11610, 1995. 4641, 4642, 4720

McCann, K. S.: The diversity–stability debate, Nature, 405, 228–233, 2000. 4658

McCree, K.: An equation for the rate of respiration of white clover plants grown under controlled conditions, in: Productivity of Photosynthetic Systems; Models and Methods, edited by Setlik, I., PUDOC, Wageningen, 221–229, 1970. 4671

McGill, B. J., Enquist, B. J., Weiher, E., and Westoby, M.: Rebuilding community ecology from functional traits., Trends Ecol. Evol., 21, 178–185, 2006. 4637

McGill, B. J., Etienne, R. S., Gray, J. S., Alonso, D., Anderson, M. J., Benecha, H. K., Dornelas, M., Enquist, B. J., Green, J. L., He, F., Hurlbert, A. H., Magurran, A. E., Marquet, P. A., Maurer, B. A., Ostling, A., Soykan, C. U., Ugland, K. I., and White, E. P.: Species abundance distributions: moving beyond single prediction theories to integration within an ecological framework, Ecol. Lett., 10, 995–1015, 2007. 4645

Title Page

Abstract | Introduction

Conclusions | References

Tables | Figures

◀ | ▶

◀ | ▶

Back | Close

Full Screen / Esc

Printer-friendly Version

Interactive Discussion

McKay, M., Conover, W., and Bechman, R.: A comparison of three methods for selecting values of input variables in the analysis of output from a computer code, Technometrics, 21, 239–245, 1979. 4636

Medvigy, D., Wofsy, S. C., Munger, J. W., Hollinger, D. Y., and Moorcroft, P. R.: Mechanistic scaling of ecosystem function and dynamics in space and time: ecosystem demography model version 2, J. Geophys. Res.-Biogeo., 114, G01002, doi:10.1029/2008JG000812, 2009. 4657

Mercado, L. M., Bellouin, N., Sitch, S., Boucher, O., Huntingford, C., Wild, M., and Cox, P.: Impact of changes in diffuse radiation on the global land carbon sink, Nature, 458, 1014–1017, 2009. 4651

Millennium Ecosystem Assessment: Ecosystems and Human Well-Being: Synthesis, Island Press, Washington DC, 2005. 4629

Monsi, M. and Saeki, T.: Über den Lichtfaktor in den Pflanzengesellschaften und seine Bedeutung für die Stoffproduktion, Jpn. J. Bot., 14, 22–52, 1953. 4669, 4670

Moorcroft, P., Hurtt, G., and Pacala, S.: A method for scaling vegetation dynamics: the ecosystem demography model (ED), Ecol. Monogr., 71, 557–585, 2001. 4657

Myneni, R., Hoffman, S., Knyazikhin, Y., Privette, J. L., Glassy, J., Tian, Y., Wang, Y., Song, X., Zhang, Y., Smith, G., Lotsch, A., Friedl, M., Morisette, J., Votava, P., Nemani, R. R., and Running, S.: Global products of vegetation leaf area and fraction absorbed PAR from year one of MODIS data, Remote Sens. Environ., 83, 214–231, 2002. 4712, 4713, 4714

Myneni, R. B., Yang, W., Nemani, R. R., Huete, A. R., Dickinson, R. E., Knyazikhin, Y., Didan, K., Fu, R., Negrón Juárez, R. I., Saatchi, S. S., Hashimoto, H., Ichii, K., Shabanov, N. V., Tan, B., Ratana, P., Privette, J. L., Morisette, J. T., Vermote, E. F., Roy, D. P., Wolfe, R. E., Friedl, M. A., Running, S. W., Votava, P., El-Saleous, N., Devadiga, S., Su, Y., and Salomonson, V. V.: Large seasonal swings in leaf area of Amazon rainforests, in: Proceedings of the National Academy of Sciences of the United States of America, 104, 4820–4823, 2007. 4646

Neilson, R., Pitelka, L., Solomon, A., Nathan, R., Midgley, G., Fragoso, J., Lischke, H., and Thompson, K.: Forecasting regional to global plant migration in response to climate change, Bioscience, 55, 749–759, 2005. 4655

Norby, R., DeLucia, E., Gielen, B., Calfapietra, C., Giardina, C., King, J., Ledford, J., McCarthy, H., Moore, D., and Ceulemans, R.: Forest response to elevated CO_2 is conserved across a broad range of productivity, in: Proceedings of the National Academy of Sciences of the United States of America, 102, 18052, 2005. 4639, 4643, 4653

Ollinger, S. V., Richardson, A. D., Martin, M. E., Hollinger, D. Y., Frolking, S. E., Reich, P. B., Plourde, L. C., Katul, G. G., Munger, J. W., Oren, R., Smith, M. L., U, K. T. P., Bolstad, P. V., Cook, B. D., Day, M. C., Martin, T. A., Monson, R. K., and Schmid, H. P.: Canopy nitrogen, carbon assimilation, and albedo in temperate and boreal forests: functional relations and potential climate feedbacks, in: Proceedings of the National Academy of Sciences of the United States of America, 105, 19336–19341, 2008. 4657, 4671

Olson, R. J., Scurlock, J. M. O., Prince, S. D., Zheng, D. L., and Johnson, K. R.: NPP Multi-Biome: NPP and Driver Data for Ecosystem Model-Data Intercomparison. Data set., Tech. rep., Environmental Sciences Division, Oak Ridge National Laboratory, ORNL Distributed Active Archive Center for Biogeochemical Dynamics, Oak Ridge, TN USA, 2001. 4640, 4717

O'Malley, M. A.: The nineteenth century roots of "everything is everywhere", Nat. Rev. Microbiol., 5, 647–651, 2007. 4632

Page, S. E., Siegert, F., Rieley, J. O., Boehm, H.-D. V., Jaya, A., and Limin, S.: The amount of carbon released from peat and forest fires in Indonesia during 1997, Nature, 420, 61–65, 2002. 4650

Pielou, E. C.: The measurement of diversity in different types of biological collections, J. Theor. Biol., 13, 131–144, 1966. 4710

Potter, C., Randerson, J., Field, C., Matson, P., Vitousek, P., Mooney, H., and Klooster, S.: Terrestrial ecosystem production – a process model-based on global satellite and surface data, Global Biogeochem. Cy., 7, 811–841, 1993. 4661

Prentice, I. C., Bondeau, A., Cramer, W., Harrison, S. P., Hickler, T., Lucht, W., Sitch, S., Smith, B., and Sykes, M. T.: Dynamic global vegetation modeling: quantifying terrestrial ecosystem responses to large-scale environmental change, in: Terrestrial Ecosystems in a Changing World, edited by Canadell, J. G., Pataki, D. E., and Pitelka, L. F., Springer, Berlin, Heidelberg, 175–192, 2007. 4630

Priestley, C. and Taylor, R.: On the assessment of surface heat-flux and evaporation using large-scale parameters, Mon. Weather Rev., 100, 81–89, 1972. 4678

Prieto, I., Armas, C., and Pugnaire, F. I.: Water release through plant roots: new insights into its consequences at the plant and ecosystem level, New Phytol., 193, 830–841, 2012. 4656

Proulx, R., Wirth, C., Voigt, W., Weigelt, A., Roscher, C., Attinger, S., Baade, J., Barnard, R. L., Buchmann, N., Buscot, F., Eisenhauer, N., Fischer, M., Gleixner, G., Halle, S., Hildebrandt, A., Kowalski, E., Kuu, A., Lange, M., Milcu, A., Niklaus, P. A., Oel-

Jena Diversity DGVM

R. Pavlick et al.

Title Page

Abstract	Introduction
Conclusions	References
Tables	Figures

◄ | ►

◄ | ►

Back | Close

Full Screen / Esc

Printer-friendly Version

Interactive Discussion

mann, Y., Rosenkranz, S., Sabais, A., Scherber, C., Scherer-Lorenzen, M., Scheu, S., Schulze, E.-D., Schumacher, J., Schwichtenberg, G., Soussana, J.-F., Temperton, V. M., Weisser, W. W., Wilcke, W., and Schmid, B.: Diversity promotes temporal stability across levels of ecosystem organization in experimental grasslands, PLoS one, 5, e13382, doi:10.1371/journal.pone.0013382, 2010. 4659

Purves, D. and Pacala, S.: Predictive models of forest dynamics, Science, 320, 1452–1453, 2008. 4630

Qian, T., Dai, A., Trenberth, K. E., and Oleson, K. W.: Simulation of global land surface conditions from 1948 to 2004. Part I: forcing data and evaluations, J. Hydrometeorol., 7, 953–975, 2006. 4638

Quesada, C. A., Lloyd, J., Anderson, L. O., Fyllas, N. M., Schwarz, M., and Czimczik, C. I.: Soils of amazonia with particular reference to the rainfor sites, Biogeosciences Discuss., 6, 3851–3921, doi:10.5194/bgd-6-3851-2009, 2009. 4652

Quetier, F., Thebault, A., and Lavorel, S.: Plant traits in a state and transition framework as markers of ecosystem response to land-use change, Ecol. Monogr., 77, 33–52, 2007. 4637, 4656

Quillet, A., Peng, C., and Garneau, M.: Toward dynamic global vegetation models for simulating vegetation-climate interactions and feedbacks: recent developments, limitations, and future challenges, Environ. Rev., 18, 333–353, 2010. 4629

Raddatz, T. J., Reick, C. H., Knorr, W., Kattge, J., Roeckner, E., Schnur, R., Schnitzler, K. G., Wetzel, P., and Jungclaus, J.: Will the tropical land biosphere dominate the climate–carbon cycle feedback during the twenty-first century?, Clim. Dynam., 29, 565–574, 2007. 4673

Randerson, J. T., Hoffman, F. M., Thornton, P. E., Mahowald, N. M., Lindsay, K., Leee, Y.-H., Nevison, C. D., Doney, S., Bonan, G., Stoeckli, R., Covey, C., Running, S. W., and Fung, I. Y.: Systematic assessment of terrestrial biogeochemistry in coupled climate-carbon models, Glob. Change Biol., 15, 2462–2484, 2009. 4633, 4638, 4639, 4642, 4645, 4650, 4653, 4701

Reich, P. B., Walters, M. B., and Ellsworth, D. S.: From tropics to tundra: global convergence in plant functioning, in: Proceedings of the National Academy of Sciences of the United States of America, 94, 13730–13734, 1997. 4669

Reich, P. B., Walters, M., Ellsworth, D., Vose, J., Volin, J., Gresham, C., and Bowman, W.: Relationships of leaf dark respiration to leaf nitrogen, specific leaf area and leaf life-span: a test across biomes and functional groups, Oecologia, 114, 471–482, 1998. 4669

Title Page

Abstract | Introduction

Conclusions | References

Tables | Figures

◄ | ►

◄ | ►

Back | Close

Full Screen / Esc

Printer-friendly Version

Interactive Discussion

Reich, P. B., Hobbie, S. E., Lee, T., Ellsworth, D. S., West, J. B., Tilman, D., Knops, J. M. H., Naeem, S., and Trost, J.: Nitrogen limitation constrains sustainability of ecosystem response to CO_2, Nature, 440, 922–925, 2006. 4648

Reich, P. B., Wright, I. J., and Lusk, C. H.: Predicting leaf physiology from simple plant and climate attributes: a global GLOPNET analysis, Ecol. Appl., 17, 1982–1988, 2007. 4630, 4631

Reiss, J., Bridle, J. R., Montoya, J. M., and Woodward, G.: Emerging horizons in biodiversity and ecosystem functioning research, Trends Ecol. Evol., 24, 505–514, 2009. 4659

Reu, B., Proulx, R., Bohn, K., Dyke, J. G., Kleidon, A., Pavlick, R., and Schmidtlein, S.: The role of climate and plant functional trade-offs in shaping global biome and biodiversity patterns, Global Ecol. Biogeogr., 20, 570–581, 2010. 4632

Reu, B., Zaehle, S., Proulx, R., Bohn, K., Kleidon, A., Pavlick, R., and Schmidtlein, S.: The role of plant functional trade-offs for biodiversity changes and biome shifts under scenarios of global climatic change, Biogeosciences, 8, 1255–1266, doi:10.5194/bg-8-1255-2011, 2011. 4632

Robock, A.: The seasonal cycle of snow cover, sea ice and surface albedo, Mon. Weather Rev., 108, 267–285, 1980. 4678

Roeckner, E., Arpe, K., Bengtsson, L., Christoph, M., Claussen, M., Dümenil, L., Esch, M., Giorgetta, M., Schlese, U., and Schulzweida, U.: The Atmospheric General Circulation Model ECHAM-4: Model Description and Simulation of Present-Day Climate, Max Planck Institute for Meteorology, Hamburg, Germany, 1996. 4661, 4668, 4675

Ryan, M.: A simple method for estimating gross carbon budgets for vegetation in forest ecosystems, Tree Physiol., 9, 255–266, 1991. 4672

Ryu, Y., Baldocchi, D., Kobayashi, H., van Ingen, C., Li, J., Black, T. A., Beringer, J., van Gorsel, E., Knohl, A., Law, B. E., and Roupsard, O.: Integration of MODIS land and atmosphere products with a coupled-process model to estimate gross primary productivity and evapotranspiration from 1 km to global, Global Biogeochem., 25, GB4017, doi:10.1029/2011GB004053, 2011. 4647

Saatchi, S. S., Houghton, R. A., Alvala, R. C. D. S., Soares, J. V., and Yu, Y.: Distribution of aboveground live biomass in the Amazon Basin, Glob. Change Biol., 13, 816–837, 2007. 4643, 4651, 4723

Title Page

Abstract | Introduction

Conclusions | References

Tables | Figures

◄ | ►►

◄ | ►

Back | Close

Full Screen / Esc

Printer-friendly Version

Interactive Discussion

Samanta, A., Ganguly, S., Hashimoto, H., Devadiga, S., Vermote, E., Knyazikhin, Y., Nemani, R. R., and Myneni, R.: Amazon forests did not green-up during the 2005 drought, Geophys. Res. Lett., 37, L05401, doi:10.1029/2009GL042154, 2010. 4646

Scheiter, S. and Higgins, S. L.: Impacts of climate change on the vegetation of Africa: an adaptive dynamic vegetation modelling approach, Glob. Change Biol., 15, 2224–2246, 2009. 4631

Shinozaki, K., Yoda, K., Hozumi, K., and Kira, T.: A quantitative analysis of plant form – the pipe model theory, 1. basic analysis, Jpn. J. Ecol., 14, 97–105, 1964. 4669

Shipley, B., Lechowicz, M., Wright, I. J., and Reich, P. B.: Fundamental trade-offs generating the worldwide leaf economics spectrum, Ecology, 87, 535–541, 2006a. 4669

Shipley, B., Vile, D., and Garnier, E.: From plant traits to plant communities: a statistical mechanistic approach to biodiversity, Science, 314, 812–814, 2006b. 4638

Sitch, S., Smith, B., Prentice, I. C., Arneth, A., Bondeau, A., Cramer, W., Kaplan, J. O., Levis, S., Lucht, W., Sykes, M. T., Thonicke, K., and Venevsky, S.: Evaluation of ecosystem dynamics, plant geography and terrestrial carbon cycling in the LPJ dynamic global vegetation model, Glob. Change Biol., 9, 161–185, 2003. 4629, 4630, 4647

Sitch, S., Huntingford, C., Gedney, N., Levy, P. E., Lomas, M., Piao, S. L., Betts, R. A., Ciais, P., Cox, P., Friedlingstein, P., Jones, C. D., Prentice, I. C., and Woodward, F. I.: Evaluation of the terrestrial carbon cycle, future plant geography and climate-carbon cycle feedbacks using five Dynamic Global Vegetation Models (DGVMs), Glob. Change Biol., 14, 2015–2039, 2008. 4629, 4650

Smith, T. and Huston, M.: A theory of the spatial and temporal dynamics of plant communities, Plant Ecol., 83, 49–69, 1989. 4632

Sonnier, G., Shipley, B., and Navas, M.-L.: Plant traits, species pools and the prediction of relative abundance in plant communities: a maximum entropy approach, J. Veg. Sci., 21, 318–331, 2010. 4638

Stoeckli, R., Lawrence, D. M., Niu, G. Y., Oleson, K. W., Thornton, P. E., Yang, Z. L., Bonan, G., Denning, A. S., and Running, S. W.: Use of FLUXNET in the community land model development, J. Geophys. Res.-Biogeo., 113, G01025, doi:10.1029/2007JG000562, 2008. 4643

Swenson, N. G. and Weiser, M.: Plant geography upon the basis of functional traits: an example from Eastern North American trees, Ecology, 91, 2234–2241, 2010. 4656

Taylor, K.: Summarizing multiple aspects of model performance in a single diagram, J. Geophys. Res.-Atmos., 106, 7183–7192, 2001. 4649

Title Page

Abstract | Introduction

Conclusions | References

Tables | Figures

◀◀ | ▶▶

◀ | ▶

Back | Close

Full Screen / Esc

Printer-friendly Version

Interactive Discussion

Thonicke, K., Venevsky, S., Sitch, S., and Cramer, W.: The role of fire disturbance for global vegetation dynamics: coupling fire into a Dynamic Global Vegetation Model, Global Ecol. Biogeogr., 10, 661–677, 2008. 4650

Thornley, J.: Respiration, growth and maintenance in plants, Nature, 227, 304–305, 1970. 4671

5 Thornton, P. E., Lamarque, J.-F., Rosenbloom, N. A., and Mahowald, N. M.: Influence of carbon-nitrogen cycle coupling on land model response to CO_2 fertilization and climate variability, Global Biogeochem. Cy., 21, GB4018, doi:10.1029/2006GB002868, 2007. 4639

Thum, T., Räisänen, P., Sevanto, S., Tuomi, M., Reick, C., Vesala, T., Raddatz, T., Aalto, T., Järvinen, H., Altimir, N., Pilegaard, K., Nagy, Z., Rambal, S., and Liski, J.: Soil carbon model
10 alternatives for ECHAM5/JSBACH climate model: evaluation and impacts on global carbon cycle estimates, J. Geophys. Res., 116, G02028, doi:10.1029/2010JG001612, 2011. 4673

Tilman, D., Reich, P. B., and Knops, J. M. H.: Biodiversity and ecosystem stability in a decade-long grassland experiment, Nature, 441, 629–632, 2006. 4630, 4659

Van Bodegom, P. M., Douma, B., Witte, F. M., Ordoñez, J. C., Bartholomeus, R. P., and
15 Aerts, R.: Going beyond limitations of plant functional types when predicting global ecosystem–atmosphere fluxes: exploring the merits of traits-based approaches, Global Ecol. Biogeogr., doi:10.1111/j.1466-8238.2011.00717.x, 2011. 4631

van der Werf, G. R., Randerson, J. T., Giglio, L., Collatz, G. J., Kasibhatla, P. S., and Arel-lano Jr., A. F.: Interannual variability in global biomass burning emissions from 1997 to 2004,
20 Atmos. Chem. Phys., 6, 3423–3441, doi:10.5194/acp-6-3423-2006, 2006. 4642

van der Werf, G. R., Dempewolf, J., Trigg, S. N., Randerson, J. T., Kasibhatla, P. S., Giglio, L., Murdiyarso, D., Peters, W., Morton, D. C., Collatz, G. J., Dolman, A. J., and DeFries, R. S.: Climate regulation of fire emissions and deforestation in equatorial Asia, in: Proceedings of the National Academy of Sciences, 105, 20350–20355, 2008. 4650

25 Vieira, S., de Camargo, P. B., Selhorst, D., da Silva, R., Hutyra, L., Chambers, J. Q., Brown, I. F., Higuchi, N., dos Santos, J., Wofsy, S. C., Trumbore, S. E., and Martinelli, L. A.: Forest struc-ture and carbon dynamics in Amazonian tropical rain forests, Oecologia, 140, 468–479, 2004. 4652

Vile, D., Shipley, B., and Garnier, E.: Ecosystem productivity can be predicted from potential
30 relative growth rate and species abundance, Ecol. Lett., 9, 1061–1067, 2006. 4637, 4656

Wang, A. and Price, D. T.: Estimating global distribution of boreal, temperate, and tropical tree plant functional types using clustering techniques, J. Geophys. Res., 112, G01024, doi:10.1029/2006JG000252, 2007. 4630

Title Page

Abstract | Introduction

Conclusions | References

Tables | Figures

◀ | ▶

◀ | ▶

Back | Close

Full Screen / Esc

Printer-friendly Version

Interactive Discussion

Webb, C. T., Hoeting, J. A., Ames, G. M., Pyne, M. I., and LeRoy Poff, N.: A structured and dynamic framework to advance traits-based theory and prediction in ecology, Ecol. Lett., 13, 267–283, 2010. 4636

Westoby, M. and Wright, I. J.: Land-plant ecology on the basis of functional traits, Trends Ecol. Evol., 21, 261–268, 2006. 4632

Westoby, M., Falster, D., Moles, A., Vesk, P., and Wright, I. J.: Plant ecological strategies: some leading dimensions of variation between species, Annu. Rev. Ecol. Syst., 33, 125–159, 2002. 4630, 4669

Wigmosta, M., Vail, L., and Lettenmaier, D.: A distributed hydrology-vegetation model for complex terrain, Water Resour. Res., 30, 1665–1679, 1994. 4676

Williams, J. W. and Jackson, S. T.: Novel climates, no-analog communities, and ecological surprises, Front. Ecol. Environ., 5, 475–482, 2007. 4631, 4659

Wolf, A., Field, C. B., and Berry, J. A.: Allometric growth and allocation in forests: a perspective from FLUXNET, Ecol. Appl., 21, 1546–1556, 2011. 4658

Woodward, F. I., Lomas, M. R., Betts, R. A., Wagner, A., Mulligan, M., and Hewitt, C. N.: Vegetation-climate feedbacks in a greenhouse world, Philos. T. R. Soc. B, 353, 29–39, 1998. 4629

Wright, I. J., Reich, P. B., Cornelissen, J. H. C., Falster, D. S., Garnier, E., Hikosaka, K., Lamont, B. B., Lee, W., Oleksyn, J., Osada, N., Poorter, H., Villar, R., Warton, D. I., and Westoby, M.: Assessing the generality of global leaf trait relationships, New Phytol., 166, 485–496, 2005. 4630, 4631

Zaehle, S. and Friend, A. D.: Carbon and nitrogen cycle dynamics in the O-CN land surface model: 1. model description, site-scale evaluation, and sensitivity to parameter estimates, Global Biogeochem. Cy., 24, GB1005, doi:10.1029/2009GB003521, 2010. 4631

Zaehle, S., Friend, A. D., Friedlingstein, P., Dentener, F., Peylin, P., and Schulz, M.: Carbon and nitrogen cycle dynamics in the O-CN land surface model: 2. role of the nitrogen cycle in the historical terrestrial carbon balance, Global Biogeochem. Cy., 24, GB1006, doi:10.1029/2009GB003522, 2010. 4647

Zhao, M., Heinsch, F., Nemani, R. R., and Running, S.: Improvements of the MODIS terrestrial gross and net primary production global data set, Remote Sens. Environ., 95, 164–176, 2005. 4640, 4712, 4713, 4714, 4715, 4718

Zhao, M., Running, S. W., and Nemani, R. R.: Sensitivity of Moderate Resolution Imaging Spectroradiometer (MODIS) terrestrial primary production to the accuracy of meteorological reanalyses, J. Geophys. Res.-Biogeo., 111, G01002, doi:10.1029/2004JG000004, 2006. 4640, 4715, 4718

Table 1. Summary of the evaluation metrics and scores. Each metric (Column 1) is associated with a possible score (Column 3) based on a subjective assessment of its level of uncertainty and model-data scale mismatch. Each metric is broken in to metric components (Column 2) with associated sub-scores (Column 4). Scores are presented for JeDi-DGVM (this paper) and, for comparison, CLM-CN and CLM-CASA' (previouly evaluated in Randerson et al., 2009). The total score for each model (out of a possible score of 100) is presented at the bottom. MODIS, MODerate Resolution Imaging Spectroradiometer; EMDI, Ecosystem Model Data Intercomparison

Metric	Metric components	Score	Sub-score	JeDi-DGVM	CASA'	CN
Leaf Area Index		15		13.4	13.5	12.0
	MODIS phase		6	5.0	5.1	4.2
	MODIS maximum		5	4.7	4.6	4.3
	MODIS mean		4	3.7	3.8	3.5
Net Primary Productivity		10		8.4	8.0	8.2
	EMDI observations		2	1.5	1.5	1.6
	EMDI histogram		4	3.4	3.0	3.4
	MODIS spatial pattern		2	1.6	1.6	1.4
	MODIS zonal means		2	1.9	1.9	1.8
CO_2 seasonal cycle comparison with Globalview phase and amplitude		15		11.8	10.4	7.7
	60–90° N		6	4.9	4.1	2.8
	30–60° N		6	4.5	4.2	3.2
	EQ–30° N		3	2.5	2.1	1.7
Carbon and energy fluxes from Ameriflux		30		18.3	17.2	16.6
	Net ecosystem exchange		6	2.6	2.5	2.1
	Gross primary productivity		6	3.5	3.4	3.5
	Latent heat		9	6.6	6.4	6.4
	Sensible heat		9	5.6	4.9	4.7
Carbon stocks and transient dynamics		30		16.3	16.7	13.8
	Aboveground biomass in the Amazon Basin		10	6.7	5.3	5.0
	NPP stimulation from elevated CO_2		10	6.9	7.9	4.1
	Interannual variability of terrestrial carbon fluxes		5	2.7	3.6	3.0
	Fire variability		5	0.0	0.0	1.7
Total			100	68.2	65.7	58.4

Table C1. State variables and parameters of the plant growth module.

Symbol	Description	Value/units
	Vegetation carbon pools	
C_A	assimilates/storage carbon pool	$gC\,m^{-2}$
C_L	leaves carbon pool	$gC\,m^{-2}$
C_R	fine roots carbon pool	$gC\,m^{-2}$
C_{WL}	woody stem carbon pool	$gC\,m^{-2}$
C_{WR}	coarse roots carbon pool	$gC\,m^{-2}$
C_S	reproduction carbon pool	$gC\,m^{-2}$
	Growing conditions	
$f_{GROW,T}$	time-weighted temperature conditions	$^\circ$C
$f_{GROW,W}$	time-weighted soil moisture conditions	$0\ldots1$
$f_{GERM,W}$	time-weighted soil moisture conditions for germination	$0\ldots1$
f_{GERM}	0: no germination, 1: germination	
f_{GROW}	0: no growth, 1: growth	
τ_T	response time to temperature conditions	days
τ_W	response time to moisture conditions	days
	Allocation and germination	
A_L	allocation from storage to leaves	$0\ldots1$
A_R	allocation from storage to fine roots	$0\ldots1$
A_{WL}	allocation from storage to stem	$0\ldots1$
A_{WR}	allocation from storage to coarse roots	$0\ldots1$
A_S	allocation from storage to reproduction	$0\ldots1$
γ_{GERM}	germination fraction	$days^{-1}$
	Turnover and senescence	
τ_{tissue}	turnover times of vegetation carbon pools	days
f_{NPP}	time-weighted productivity conditions	$gC\,m^{-2}\,days^{-1}$
τ_{NPP}	response time to productivity conditions	days
f_{SEN}	0: no senescence, 1: senescence	
	Carbon fluxes	
GERM	germination	$gC\,m^{-2}\,days^{-1}$
GPP	gross primary productivity	$gC\,m^{-2}\,days^{-1}$
RES_a	autotrophic respiration	$gC\,m^{-2}\,days^{-1}$
NPP	net primary productivity	$gC\,m^{-2}\,days^{-1}$

Jena Diversity DGVM

R. Pavlick et al.

Discussion Paper | Discussion Paper | Discussion Paper | Discussion Paper | Discussion Paper

Title Page

Abstract | Introduction

Conclusions | References

Tables | Figures

|◄ | ►|

◄ | ►

Back | Close

Full Screen / Esc

Printer-friendly Version

Interactive Discussion

Table C2. Summary of the functional trait (FT) parameters. This table summarizes the parameters in the model description which define a plant growth strategy. Column 2 gives a brief description of the effect of this parameter on the plant behaviour and column 3 gives the equation in which the parameter occurs. All of these parameters range between zero and one.

Parameter	Description	Equation
t_1	growth response time to moisture conditions	(A2)
t_2	growth response time to temperature conditions	(A2)
t_3	critical temperature for growth	(A3)
t_4	germination fraction	(A4)
t_5	allocation to reproduction	(A5)
t_6	allocation to aboveground growth	(A5)
t_7	allocation to belowground growth	(A5)
t_8	allocation to storage	(A5)
t_9	relative allocation to aboveground structure	(A5)
t_{10}	relative allocation to belowground structure	(A5)
t_{11}	turnover time of structural pools	(A6)
t_{12}	turnover time of leaf and fine root pools	(A7)
t_{13}	senescence response time to productivity conditions	(A8)
t_{14}	relative senescence aboveground	(A9)
t_{15}	plant nitrogen status	(A17)

Table C3. Parameters and state variables of the interface between the land-surface module and the plant growth module.

Symbol	Description	Value/units
	Land-surface parameters needed by land-surface module	
LAI	leaf area index, depends on C_L	$m^2 m^{-2}$
f_{VEG}	fractional vegetation cover	$0 \ldots 1$
f_{FOR}	fractional forest cover	$0 \ldots 1$
a_{ns}	snow-free surface albedo	$0 \ldots 1$
W_{MAX}	maximum plant available soil water storage, depending on C_{WR}	mm
S	potential supply rate for transpiration, depending on C_R	$mm\,days^{-1}$
	Conversion parameters	
SLA	specific leaf area, depends on τ_L, converts C_L to LAI	$m^2 gC^{-1}$
c_{WLMAX}	conversion factor for C_L to W_{LMAX}	$0.2\,mm\,m^{-2}$
c_{FOR}	conversion factor for C_{WL} to f_{FOR}	$0.002\,m^2 gC^{-1}$
a_{VEG}	canopy albedo	$0 \ldots 1$
a_{SOIL}	bare soil albedo	0.2
$W_{MAX,0}$	minimum value of W_{MAX}	$50\,mm$
c_{PAW}	unit plant available water capacity	$mm\,H_2O\,mm^{-1}\,soil$
k	light extinction coefficient	0.5
c_{SRL}	specific coarse root length, relates C_R to W_{MAX}	$2250\,mm\,gC^{-1}$
c_{SRU}	specific root water uptake, relates C_R to S	$0.5\,mm\,gC^{-1}\,days^{-1}$

Table C4. Variables and parameters used in net primary productivity calculations.

Symbol	Description	Value/units
h	day length	s
θ	convexity of photosynthesis-radiation curve	0.9
ϕ	photosyntheic quantum efficiency	$2.73\,\mu\mathrm{gC\,J^{-1}}$
I_a	absorbed photosynthetically active radiation	$\mathrm{W\,m^{-2}}$
P_max	light-saturated photosynthetic rate	$\mathrm{gC\,m^{-2}\,s^{-1}}$
$[N_\mathrm{L}]$	canopy nitrogen concentration	$\mathrm{gN\,gC^{-1}}$
α_T	temperature limitation on productivity	$0\ldots1$
$\alpha_\mathrm{H_2O}$	water limitation on productivity	$0\ldots1$
$c_\mathrm{RES,tissue}$	growth respiration coefficient	$\mathrm{gC\,gC^{-1}}$
$c_\mathrm{RES,N}$	maintenance respiration coefficient	$\mathrm{gC\,gN^{-1}}$
$Q_\mathrm{10,AR}$	temperature sensitivity of autotrophic respiration	1.6

Table C5. State variables, fluxes, and parameters of the soil carbon module.

Symbol	Description	Value/units
	Detritus carbon pools	
C_{LIT}	fine litter carbon pool	$gC\,m^{-2}$
C_{CWD}	woody litter carbon pool	$gC\,m^{-2}$
C_{SOIL}	soil carbon pool	$gC\,m^{-2}$
	Carbon fluxes	
$\langle LIT_{tissue}\rangle$	community-aggregated litter fluxes	$gC\,m^{-2}\,days^{-1}$
DEC_x	decomposition fluxes from the detritus carbon pools	$gC\,m^{-2}\,days^{-1}$
$\langle GPP\rangle$	community-aggregated gross primary productivity	$gC\,m^{-2}\,days^{-1}$
$\langle RES_a\rangle$	community-aggregated autotrophic respiration	$gC\,m^{-2}\,days^{-1}$
RES_h	heterotrophic respiration	$gC\,m^{-2}\,days^{-1}$
NEE	net ecosystem exchange	$gC\,m^{-2}\,days^{-1}$
	Parameters	
$c_{lit\triangleright atm}$	fraction of fine litter decomposition to atmosphere	0.77
$c_{cwd\triangleright atm}$	fraction of woody litter decomposition to atmosphere	0.2
τ_{LIT}	turnover time of fine litter at 20 °C	2.05 yr
τ_{CWD}	turnover time of woody litter at 20 °C	60 yr
τ_{SOIL}	turnover time of soil carbon at 20 °C	100 yr
$Q_{10,HR}$	heterotrophic respiration coefficient	1.4

Table C6. Forcing, state, and flux variables of the land-surface module.

Symbol	Description	Value/units
	Forcing variables	
P	precipitation	$mm\,days^{-1}$
$R_{sw\downarrow}$	downwelling shortwave radiation	$W\,m^{-2}$
$R_{lw\downarrow}$	downward longwave radiation	$W\,m^{-2}$
T	2 m air temperature	$^\circ C$
	Water pools	
W_S	water stored in snow cover	mm
W_L	water intercepted in canopy	mm
W	water stored in rooting zone	mm
W_{SUB}	water stored below rooting zone	mm
	Water fluxes	
P_{snow}	snowfall	$mm\,days^{-1}$
P_{rain}	rainfall	$mm\,days^{-1}$
F_{melt}	snow melt	$mm\,days^{-1}$
F_{thfall}	throughfall	$mm\,days^{-1}$
F_{runoff}	runoff	$mm\,days^{-1}$
F_{drain}	drainage from rooting zone	$mm\,days^{-1}$
$F_{\Delta Wmax}$	flux due to change in rooting zone depth	$mm\,days^{-1}$
$F_{subdrain}$	drainage from sub-rooting zone	$mm\,days^{-1}$
E_{bare}	bare soil evaporation	$mm\,days^{-1}$
E_{can}	evaporation from the canopy reservoir	$mm\,days^{-1}$
E_{snow}	sublimiation from snow cover	$mm\,days^{-1}$
E_{trans}	transpiration	$mm\,days^{-1}$

Table C7. Other parameters and variables of the land-surface module.

Symbol	Description	Value/units
	Drainage parameters	
d_{min}	slow drainage rate	$0.24\,\text{mm days}^{-1}$
d_{max}	fast drainage rate	$2.4\,\text{mm days}^{-1}$
d	drainage exponent	1.5
W_{SUBmax}	maximum storage capacity of the entire soil column	1500 mm
	Snow cover parameters	
$a_{s,min}$	minimum snow albedo	$0.4, \ldots, 0.8$
$a_{s,max}$	maximum snow albedo	$0.3, \ldots, 0.4$
a_s	snow albedo	$0.3, \ldots, 0.8$
$W_{S,crit}$	critical snow depth	10 mm
f_{SNOW}	fractional snow area	$0 \ldots 1$
	Evapotranspiration parameters and variables	
ϵ	average emissivity of land surfaces	0.97
σ	Stefan-Boltzmann constant	$5.6703 \cdot 10^{-8}\,\text{W m}^{-2}\,\text{K}^{-4}$
α_p	Priestly-Taylor coefficient	1.26
$\epsilon(T)$	slope of the saturation-vapour pressure curve	Pa K^{-1}
Γ	psychrometric constant	$65\,\text{Pa K}^{-1}$
λ	latent heat of vaporization for water	$2500\,\text{J kg}^{-1}$
$R_{net,s}$	net radiation on snow-covered areas	J days^{-2}
$R_{net,ns}$	net radiation on snow-free areas	J days^{-2}
D_s	potential evapotranspiration from snow-covered areas	mm days^{-1}
D_{ns}	potential evapotranspiration from snow-free areas	mm days^{-1}
W_{top}	bare soil evaporation depth	50 mm
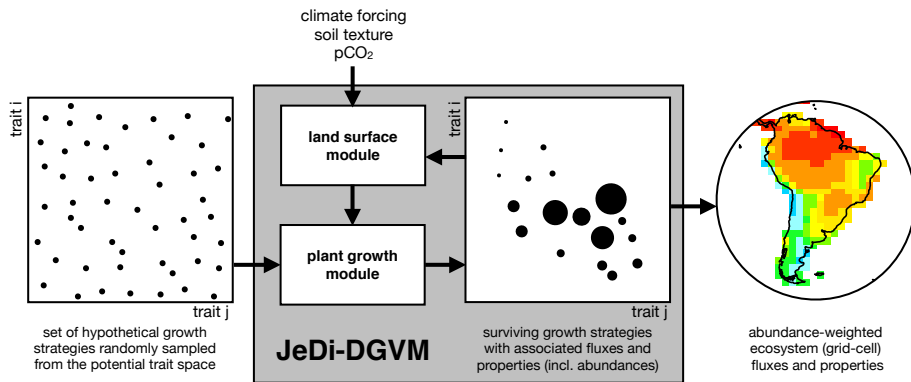
Fig. 1. Schematic diagram of the JeDi-DGVM modelling approach. The model generates a large number of hypothetical plant growth strategies, each defined by 15 functional trait parameters that characterize plant behavior with regards to carbon allocation, phenology, and ecophysiology. The trait parameter values are randomly sampled from their full observed or theoretical ranges. The plant growth module simulates the development of the plant growth strategies (independently and in parallel) based on fundamental ecophysiological processes (e.g. photosynthesis, respiration, allocation, phenology, and turnover). The environmental conditions of each strategy are provided by the land surface module, which simulates canopy interception, infiltration, evaporation, root water uptake, and runoff using daily meteorological forcings of downwelling shortwave and longwave radiation, air temperature and precipitation. Land-surface parameters (e.g. leaf area index, surface albedo, and rooting depth) derived from the carbon pools and trait parameters of each plant growth strategy affect its simulated land-surface hydrology and, consequently, its net primary productivity (NPP), i.e. its supply of assimilates. Functional trade-offs and the climatic conditions in each grid cell constrain the range and relative fitness of the surviving growth strategies (i.e. those that are able to maintain a positive balance of stored assimilates). The fluxes and properties of the surviving plant growth strategies are averaged, weighted by their relative biomasses, at each time step and grid cell to produce aggregated ecosystem-scale output variables. The aggregated litter fluxes form the input for an additional module (not shown) for simulating soil carbon dynamics and heterotrophic respiration.

Title Page

Abstract | Introduction

Conclusions | References

Tables | Figures

◄ | ►

◄ | ►

Back | Close

Full Screen / Esc

Printer-friendly Version

Interactive Discussion
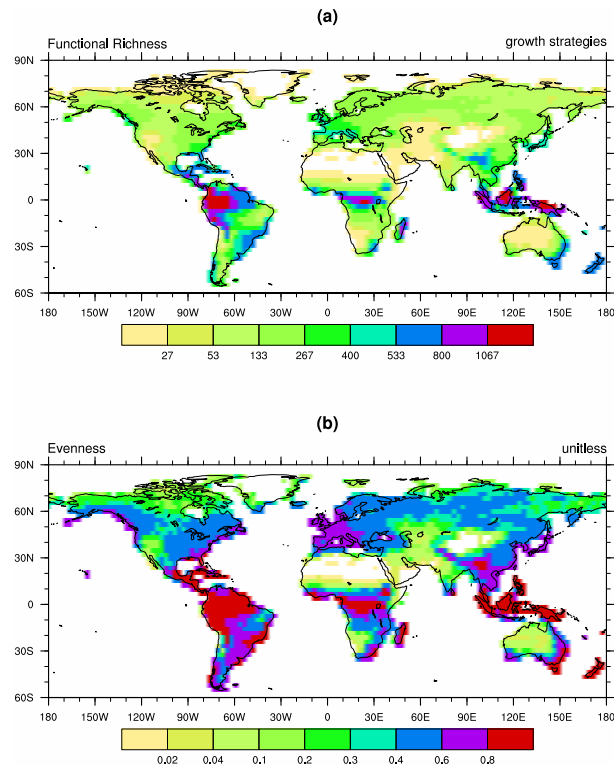
Fig. 2. Geographic patterns of **(a)** richness and **(b)** community evenness as simulated by JeDi-DGVM. Richness is simply the number of surviving plant growth strategies in a grid cell out of the 2000 tested plant growth strategies. Community evenness is calculated as $\frac{H'}{H_{max}'}$, where H' is the Shannon entropy of the abundance distribution in a grid cell and H_{max}' is the maximum possible value of H' if all growth strategies were equally abundant (Pielou, 1966).
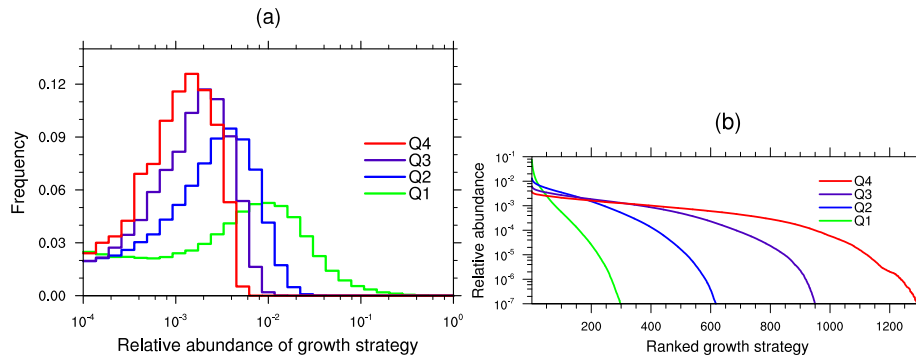
Fig. 3. (a) Simulated relative abundance distributions of plant growth strategies for four richness quartiles. **(b)** Simulated relative abundance versus growth strategy rank for four richness quartiles. On the x-axis, growth strategies are ranked according to their abundances, which in turn are plotted on the y-axis. The relative abundance distributions are averaged over all grid points falling into four classes of functional richness: grid points with low richness (Q1; $0 < D > 0.25$ of the maximum simulated richness level) to medium (Q2; $0.25 < D > 0.50$), high (Q3; $0.50 < D > 0.75$) and very high richness (Q4; $0.75 < D > 1.00$), where the richness D is expressed in relation to the grid cell with maximum simulated value of functional richness.

Discussion Paper | Discussion Paper | Discussion Paper | Discussion Paper

Title Page

Abstract | Introduction

Conclusions | References

Tables | Figures

◄ | ►

◄ | ►

Back | Close

Full Screen / Esc

Printer-friendly Version

Interactive Discussion
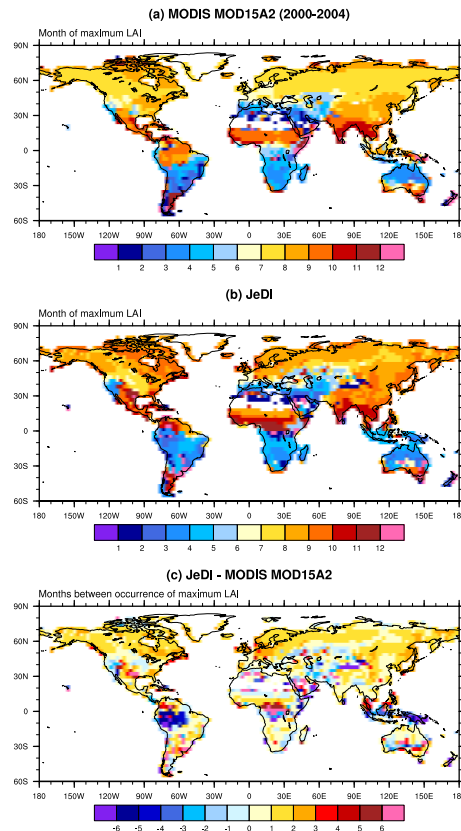
Fig. 4. Mean month of maximum leaf area index for years 2000–2004 from **(a)** MODIS MOD15A2 Collection 4 LAI product (Myneni et al., 2002; Zhao et al., 2005); **(b)** as simulated by JeDi-DGVM; and **(c)** the lag in months between the occurrence of maximum LAI in the MODIS observations and the JeDi-DGVM model output.
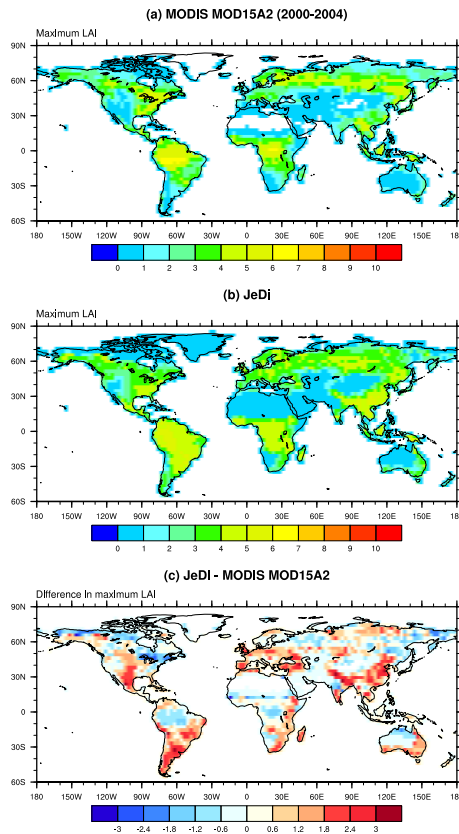
Fig. 5. Mean intra-annual maximum leaf area index for years 2000–2004 from **(a)** MODIS MOD15A2 Collection 4 LAI product (Myneni et al., 2002; Zhao et al., 2005); **(b)** as simulated byJeDi-DGVM; and **(c)** the difference between the MODIS observations and the JeDi-DGVM model output.

Title Page

Abstract | Introduction

Conclusions | References

Tables | Figures

◄◄ | ►►

◄ | ►

Back | Close

Full Screen / Esc

Printer-friendly Version

Interactive Discussion
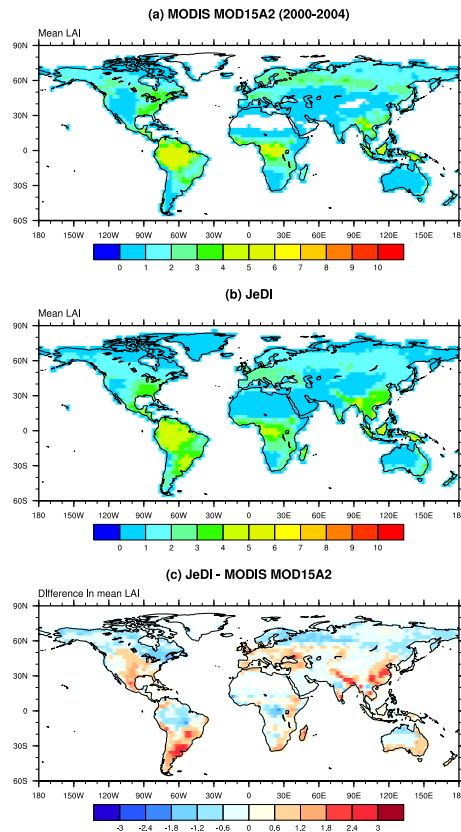
Fig. 6. Mean leaf area index for years 2000–2004 from **(a)** MODIS MOD15A2 Collection 4 LAI product (Myneni et al., 2002; Zhao et al., 2005); **(b)** as simulated by JeDi-DGVM; and **(c)** the difference between the MODIS observations and the JeDi-DGVM model output.
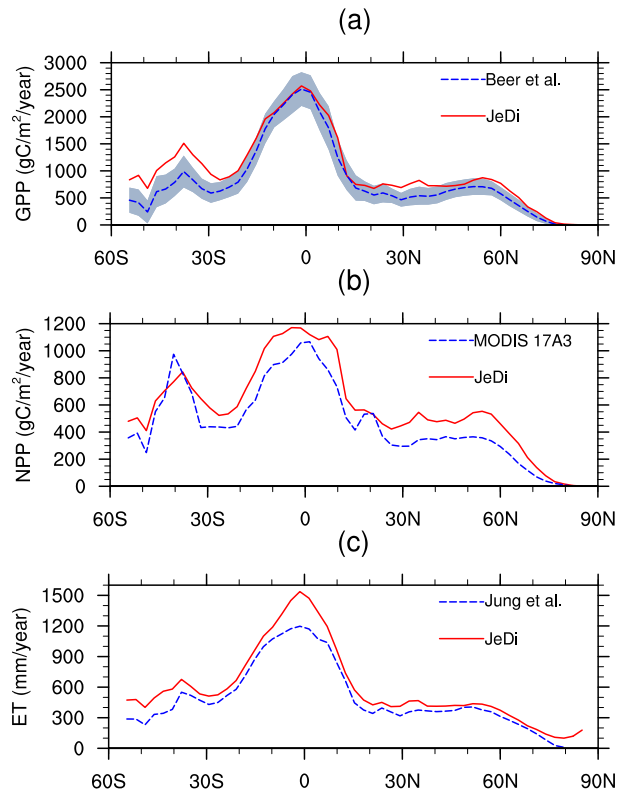
Fig. 7. Comparison of mean annual zonally-averaged fluxes as simulated by JeDi-DGVM with **(a)** observation-based estimates of gross primary productivity (Beer et al., 2010); **(b)** net primary productivity from the MODIS MOD17A3 Collection 4.5 product (Heinsch et al., 2006; Zhao et al., 2005, 2006); and **(c)** observation-based estimates of evapotranspiration (Jung et al., 2010). The blue-shaded region in **(a)** represents the median absolute deviation of the five diagnostic models used in producing the observation-based estimate.
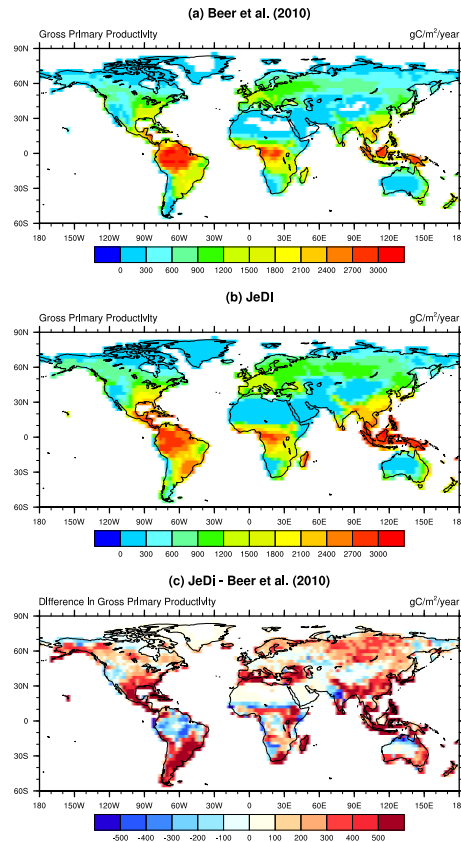
Fig. 8. (a) Observation-based estimate of mean annual gross primary productivity for years 1998–2005 (Beer et al., 2010); **(b)** mean annual terrestrial gross primary productivity from JeDi-DGVM for years 1998–2004; and **(c)** the difference between the observation-based estimate and the JeDi-DGVM model output.

Title Page

Abstract | Introduction

Conclusions | References

Tables | Figures

◄ | ►

◄ | ►

Back | Close

Full Screen / Esc

Printer-friendly Version

Interactive Discussion
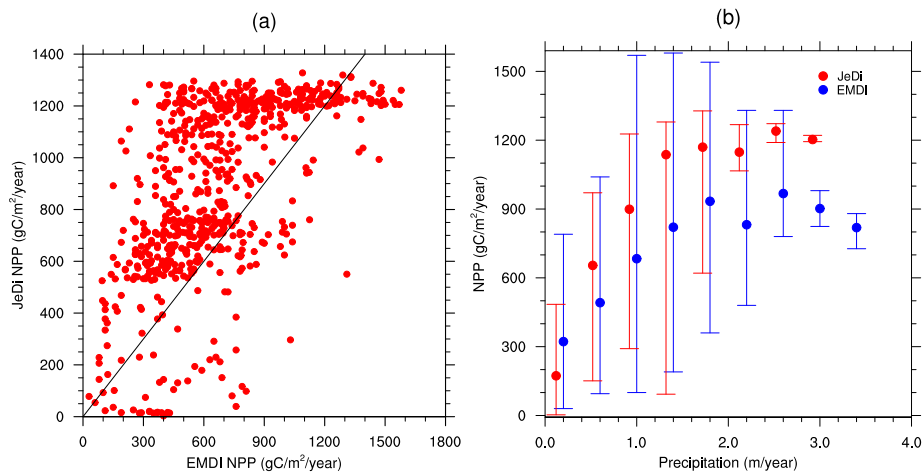
Fig. 9. Comparison of net primary productivity between JeDi-DGVM model output (mean over years 1975–2000) and 933 site observations from the Ecosystem Model Data Intercomparison Initiative (EMDI) class B dataset (Olson et al., 2001). Shown as **(a)** scatterplot where the red dots represent matched pairs of model grid cells and observation sites and the black line is a 1 : 1 line; and **(b)** the same but normalized by precipitation (binned in to 400 mm yr^{-1} increments).
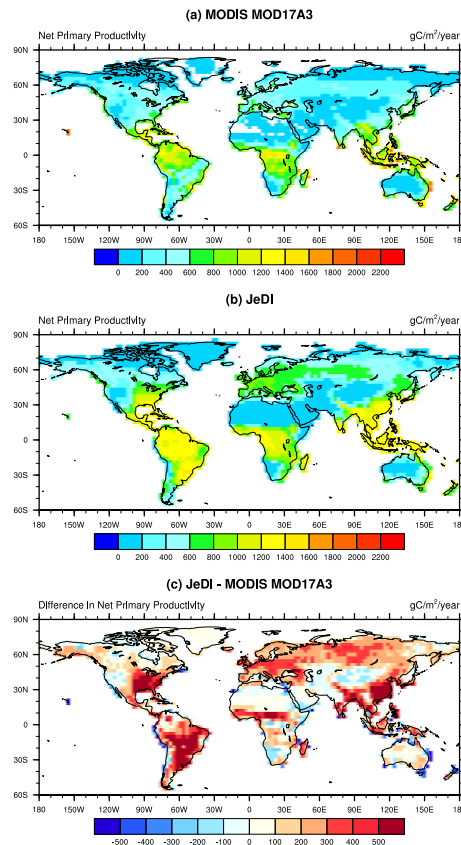
Fig. 10. Mean annual net primary productivity for years 2000–2004 from **(a)** MODIS MOD17A3 Collection 4.5 product (Heinsch et al., 2006; Zhao et al., 2005, 2006); **(b)** as simulated by JeDi-DGVM; and **(c)** the difference between the MODIS product and the JeDi-DGVM model output.
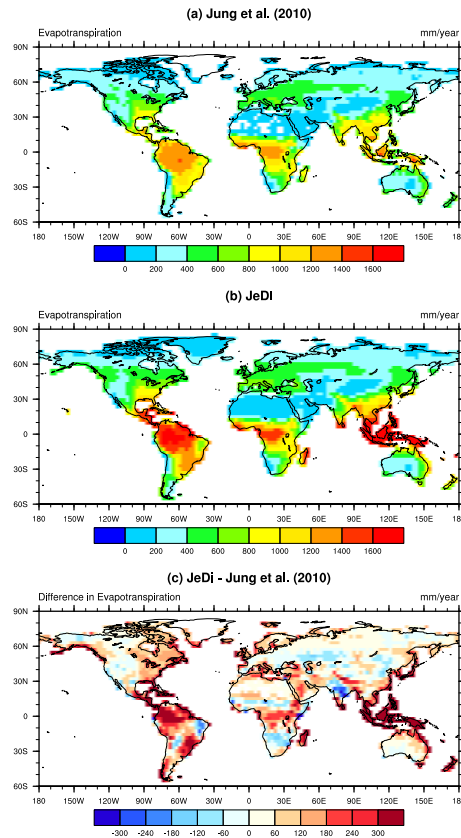
Fig. 11. (a) Observation-based estimate of mean annual evapotranspiration for years 1982–2008 (Jung et al., 2010); **(b)** mean annual gross primary productivity as simulated by JeDi-DGVM for years 1982–2004; and **(c)** the difference between the observation-based estimate and the JeDi-DGVM model output.
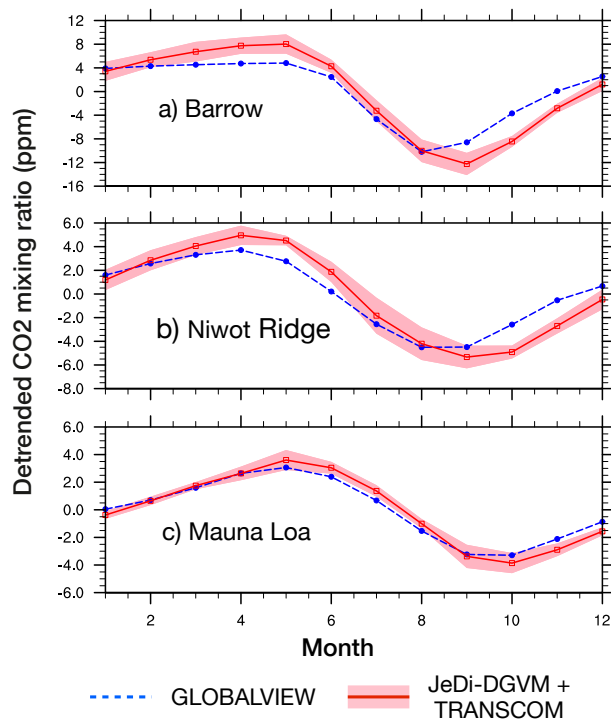
Fig. 12. Mean seasonal cycle of atmospheric CO_2 at **(a)** Barrow, Alaska (71° N), **(b)** Niwot Ridge, Colorado (40° N), **(c)** Mauna Loa, Hawaii (20° N) for years 1991–2000. The dashed blue lines represent the observations from the GLOBALVIEW dataset (Masarie and Tans, 1995). The JeDi-DGVM estimates were obtained by combining the simulated NEE fluxes with the monthly impulse response functions (Gurney et al., 2004) of the 13 TRANSCOM atmospheric tracer transport models. The red line represents the mean of the model estimates. The light red shaded region represents one standard deviation around the multimodel mean.
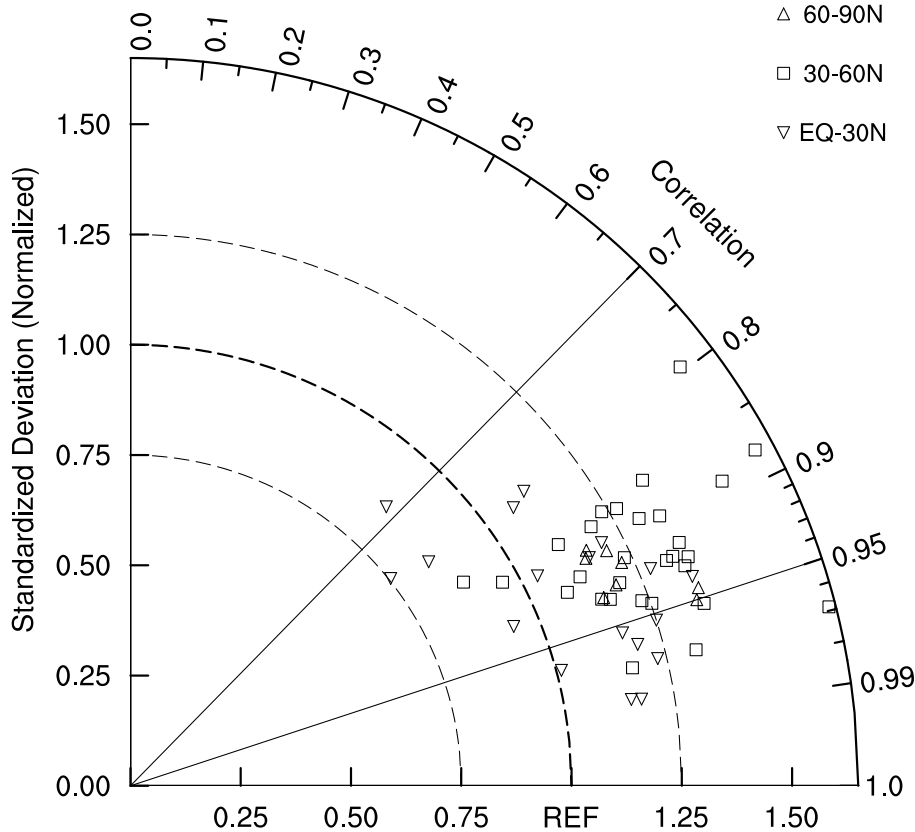
Fig. 13. Taylor diagram comparing the simulated mean annual cycle of atmospheric CO_2 for years 1991–2000 to GLOBALVIEW observations at 57 stations in the Northern Hemisphere. The annual cycle of atmospheric CO_2 was computed by applying TRANSCOM impulse response functions (Gurney et al., 2004) to the monthly NEE fluxes simulated by JeDi-DGVM.

Title Page

Abstract | Introduction

Conclusions | References

Tables | Figures

⏮ | ⏭

◄ | ►

Back | Close

Full Screen / Esc

Printer-friendly Version

Interactive Discussion
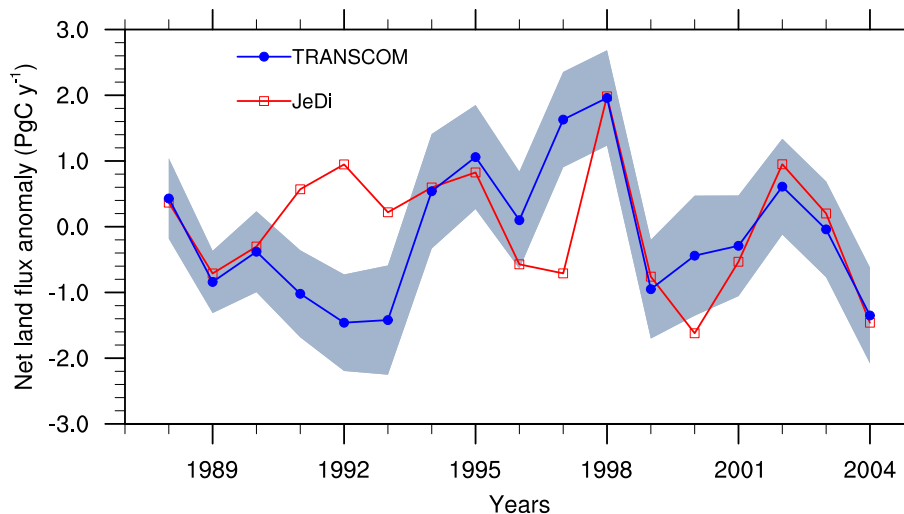
Fig. 14. Comparison of the interannual variability in the global land net ecosystem exchange fluxes from the JeDi-DGVM to the TRANSCOM atmospheric model inversion estimates (Baker et al., 2006) for years 1988–2004. The red line represents the JeDi-DGVM flux anomalies from the long-term mean. The blue line represents the mean of the 13 models from the TRANSCOM experiment after removing the seasonal cycle and the long-term mean for each model. The light blue shaded region represents 1 standard deviation around the TRANSCOM multimodel mean.
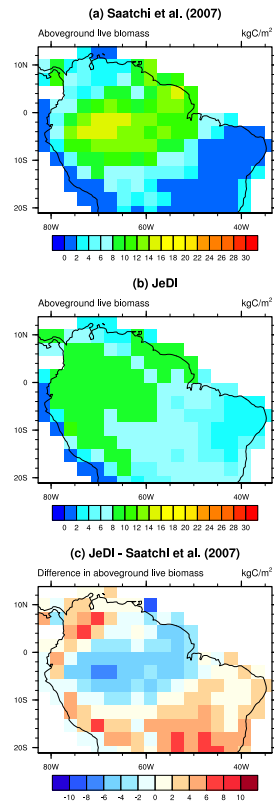
Fig. 15. Aboveground live biomass in the Amazon Basin from **(a)** observation-based estimates using plot measurements and remote sensing data (Saatchi et al., 2007); **(b)** as simulated by JeDi-DGVM at model year 2000; and **(c)** the difference between the observation-based estimates and the JeDi-DGVM model output.
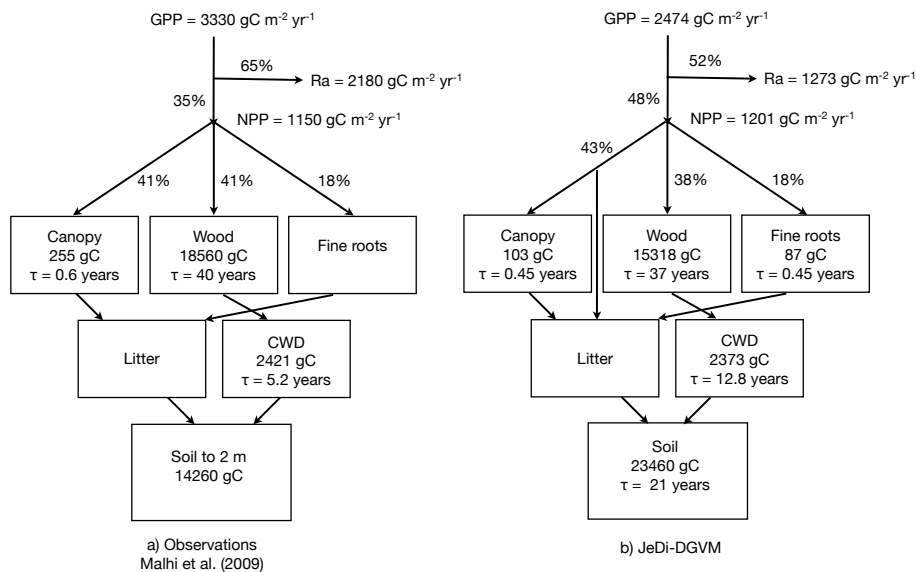
Fig. 16. Carbon pools and fluxes in Amazonia from **(a)** synthesis of observations (Malhi et al., 2009) and **(b)** as simulated by JeDi-DGVM for years 1980–2004. GPP, gross primary productivity; R_a, autotrophic respiration; NPP, net primary productivity; CWD, coarse woody debris.
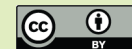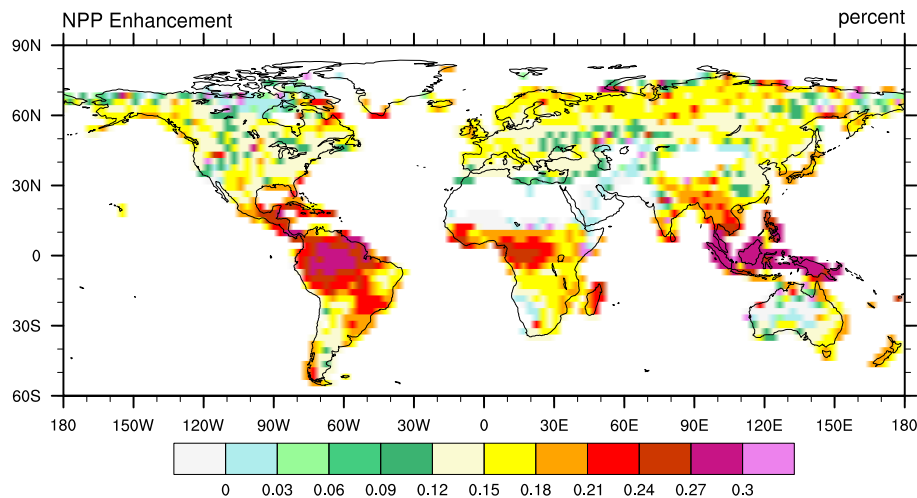
Fig. 17. Geographic pattern of the simulated enhancement of net primary productivity (NPP) due to a step increase of atmospheric CO_2 concentrations from ambient to 550 ppm. NPP values averaged over the period 1997–2001.
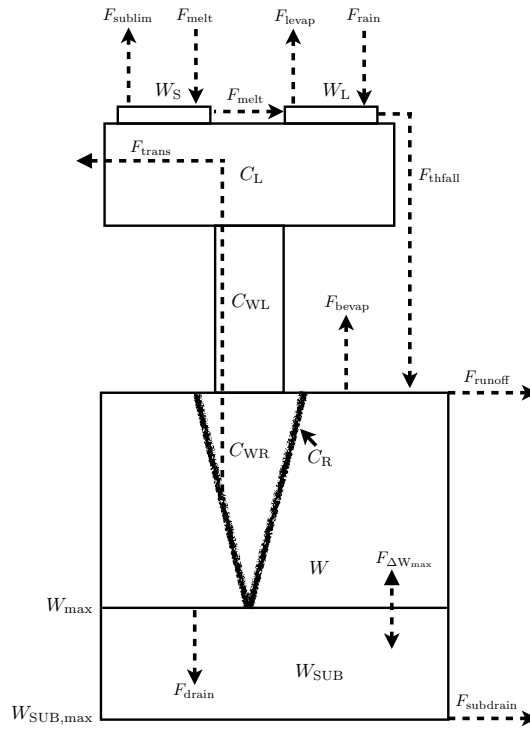
Fig. 18. Schematic diagram of the land-surface module. For symbols, see Tables C1, C3, C6, and C7.

Title Page

Abstract | Introduction

Conclusions | References

Tables | Figures

|◄ | ►|

◄ | ►

Back | Close

Full Screen / Esc